Associated absorption in radio quasars. I. C IV absorption and the growth of radio sources

Joanne C. Baker[1,2,3], Richard W. Hunstead[4], Ramana M. Athreya[5,6], Peter D. Barthel[7], Eric de Silva[3],
Matthew D. Lehnert[8], Richard D.E. Saunders[3]

ABSTRACT

We assess the global properties of associated C IV$\lambda\lambda$1548,1550 absorption lines measured in the spectra of radio-loud quasars drawn from a near-complete, low-frequency selected sample. The observations span restframe C IV in two redshift ranges — $0.7 < z < 1.0$ and $1.5 < z < 3.0$ — which were targetted in the UV with HST/STIS and in the optical with ground-based telescopes, respectively. First, we corroborate trends for C IV associated absorption to be found preferentially in steep-spectrum and lobe-dominated quasars, implying the absorbing material tends to lie away from the radio-jet axis. Furthermore, we find a clear anticorrelation between C IV absorption strength and the projected linear size of steep-spectrum quasars, indicative of an evolutionary sequence. We also find that heavily-absorbed quasars are systematically redder, implying dust is mixed in with the C IV-absorbing gas. No redshift dependence was found in any of the trends considered. These new results show that radio sources are triggered in galaxies which are exceptionally rich in gas and dust, which then dissipates on a timescale comparable with, but less than, that of the radio source. This observational sequence, together with the lack of redshift-dependence, points to a direct causal link between the event which triggered the radio source and the build-up of absorbing gas and dust, whose make-up is tantalisingly similar to the products of a post-merger starburst. Thus, these new results provide direct evidence for the clearing of absorbing material around quasars with time, as well as the probable association of starburst activity with the onset of the radio activity in AGN.

Subject headings: Galaxies: active — quasars: general — quasars: absorption lines

[1]Hubble Fellow.
[2]Astronomy Department, 601 Campbell Hall, University of California, Berkeley, CA 94720, USA.
[3]Astrophysics, Cavendish Laboratory, Madingley Road, Cambridge, CB3 0HE, UK.
[4]School of Physics, University of Sydney, NSW 2006, Australia.
[5]Institut d'Astrophysique de Paris, 98bis Boulevard Arago, 75014 Paris, France.
[6]European Southern Observatory, Casilla 19001, Santiago 19, Chile.
[7]Kapteyn Institute, Postbus 800, 9700 AV Groningen, The Netherlands
[8]Max-Planck-Institut für Extraterrestrische Physik, Postfach 1312, 85741 Garching, Germany.

1. Introduction

Quasar absorption lines provide a unique and powerful tool for probing tenuous gas clouds throughout the universe. The physical regimes probed in absorption differ from those which dominate the emission of both galaxies and Active Galactic Nuclei (AGN), and hence absorption provides a complementary view of the material composition of galaxies and AGN. Consequently, absorption lines occurring very close to the quasar emission-line redshift — associated absorbers — are valuable probes of local quasar environments, potentially intercepting gas from a range of locations along the sightline. For instance, absorption can arise in gas flows near the quasar central engine, the interstellar medium (ISM) of the quasar host galaxy, or the ISM of neighbouring galaxies which may themselves be in clusters or groups.

Associated absorption systems (usually defined by an absorption redshift, z_a, lying within $5000\,\mathrm{km\,s^{-1}}$ of the emission-line redshift, z_e) seem to be more numerous than can be accounted for by randomly distributed galaxies along the quasar sightline (Weymann et al. 1979; Foltz et al. 1986, 1988; Richards et al. 1999, 2001 and references therein; but see e.g. Young, Sargent & Boksenberg 1982). The absorption systems occur most frequently in radio-loud quasars, especially those with steep radio spectra (Anderson et al. 1987; Foltz et al. 1988; Richards et al. 1999, 2001), favouring a direct link with AGN activity and also, perhaps, the processes of radio-jet formation.

Many $z_\mathrm{a} \approx z_\mathrm{e}$ absorbers also differ subtly in ionisation or velocity profiles from those seen along sightlines traversing normal galaxy halos, suggesting $z_\mathrm{a} \approx z_\mathrm{e}$ absorbing clouds experience directly the hard radiation field and kinematics of the AGN (Petitjean, Rauch & Carswell 1994; Hamann & Ferland 1999; Hamann et al. 2001). In the most extreme cases, very broad absorption-lines (BALs; FWHMs of thousands of $\mathrm{km\,s^{-1}}$) are seen (see summaries by Turnshek et al. 1988; Turnshek 1995; Weymann 1995). These broad troughs are probably due to outflowing, dense winds close to the nucleus. Interestingly, BAL systems occur almost exclusively in radio-quiet quasars (but see Becker et al. 1997, 2000; Gregg et al. 2000). This paper, however, will focus exclusively on the narrow associated absorption-line systems (FWHMs tens to hundreds of $\mathrm{km\,s^{-1}}$).

Among radio-loud quasars, the trend for $z_\mathrm{a} \approx z_\mathrm{e}$ absorption to occur preferentially in steep-spectrum and lobe-dominated quasars (Barthel, Tytler & Vestergaard 1997) can be interpreted within the basic framework of the 'unified schemes' for AGN as an orientation effect. Steep-spectrum radio sources are thought to be viewed at large angles, θ, to the radio-jet axis, and the presence of absorbing material is consistent with the basic geometry of an obscuring torus which blocks the nuclear light from the observer beyond a viewing angle of about $\theta \sim 45°$(see Barthel 1989; Antonucci 1993; Urry & Padovani 1995). In practice, considerable amounts of obscuring material must also lie within the torus opening angle, to cause the optical reddening seen even in steep-spectrum quasars (Baker & Hunstead 1995; Baker 1997).

All properties of the AGN population cannot, however, be explained in terms of viewing angle differences alone. For example, 20–30% of *compact* radio sources (angular sizes $< 2''$) have steep rather than flat spectra, implying their radio jets are not beamed strongly towards us. Therefore, the projected sizes of compact, steep-spectrum (CSS) sources are not small simply because their jets are oriented close to our line of sight, but rather they are intrinsically small (see Fanti et al. 1990). In fact, as a class, CSS sources (see review by O'Dea 1998) do obey the orientation-unification picture (e.g. Saikia et al. 2001), but they comprise intrinsically small versions of the larger radio-source population, their luminous radio emission emanating from regions within the envelope of the host galaxy. The majority of CSS sources are thought to be young, and presumably will grow into large-scale sources (Readhead et al. 1996; Owsianik & Conway 1998; Taylor et al. 2000; Saikia et al. 2001; de Silva et al., 2001, in preparation). Therefore source evolution must also be folded into AGN studies. However, apart from the evolution of the radio components, which has been extensively modelled, little is known about evolution of individual quasars at other wavelengths.

To build up a picture of how the absorbing material is distributed around quasars, or its rate of occurrence among different types of quasar, necessitates sampling many sightlines over a wide range of viewing angles to the nucleus. Therefore, it is crucial to use complete and unbiased samples for such an investigation. Unfortunately, most previous work was based on heterogeneous samples. In this paper, we investigate associated C IV absorption in a complete sample of low-frequency selected quasars. Using new optical spectra at moderate resolution (1–3Å), we focus

initially on the C IV$\lambda\lambda$1548,1550 absorption doublet for a basic assessment of absorption characteristics. Spectra of the entire Ly α to C IV restframe region and further analysis will be presented in a second paper (Paper II). To test for any redshift dependence of the absorbers (e.g. Ganguly et al. 2001), quasars were observed in two redshift ranges — (i) $1.5 < z < 3.0$, where Ly α and C IV are observable from the ground, and (ii) $0.7 < z < 1.0$, where Ly α and C IV have been observed with STIS on HST. CSS quasars are included in this study — we define them as having linear sizes less than $D = 25$ kpc (measured between the outer radio hotspots) and a steep spectrum ($\alpha > 0.5$; where $S_\nu \propto \nu^{-\alpha}$) as observed between 408 MHz and 4.86 GHz (see Kapahi et al. 1998). We also define the orientation-dependent ratio, R, to be the ratio of core to lobe luminosity measured at a rest-frame frequency of 10 GHz (see Kapahi et al. 1998). For consistency with earlier papers we use cosmological parameters $H_0 = 50\,\mathrm{km\,s^{-1}Mpc^{-1}}$, $q_0 = 0.5$ and $\Lambda = 0$ throughout. We note that, over the redshift range under consideration, the resulting linear sizes are consistent to within 10% of the values using current best estimates for cosmological parameters (namely $\Omega_m = 0.3$, $\Omega_\Lambda = 0.7$, $H_0 = 70\,\mathrm{km\,s^{-1}Mpc^{-1}}$).

2. Observations

2.1. The Parent Sample

The quasars are all drawn from the well-defined Molonglo Quasar Sample (MQS; Kapahi et al. 1998). Briefly, the MQS comprises all quasars brighter than $S_{408} = 0.95$ Jy in the $-30^\circ < \delta < -20^\circ$ Declination strip (excluding low Galactic latitudes, $|b| < 20^\circ$) of the 408-MHz Molonglo Reference Catalogue (MRC; Large et al. 1981). Optical identifications for all 557 MRC radio sources in the strip above this flux-density limit have been obtained, and 111 quasars (including 6 BL-Lacs) have been identified following spectroscopy. Redshifts of the quasars span the range $0.1 < z < 3.0$. Due to its careful selection the MQS is estimated to be more than 97% complete, with no optical magnitude limit, and is also relatively unbiased in terms of radio-jet orientation, as isotropic components dominate the radio emission at 408 MHz. Full details of the sample selection, and radio images, are given by Kapahi et al. (1998), and the initial low-resolution optical spectroscopy is presented by Baker et al. (1999), to which the reader is referred. To study associated absorption systems in the quasars, additional spectroscopy of the restframe Ly α to C IV region has been sought for two redshift-limited sub-samples, described below. Tables 1 and 2 list these low- and high-redshift sub-samples, together with basic radio and optical properties and observational details.

2.2. Ground-based spectroscopy of $z \sim 2$ quasars

A program of moderate-resolution (1–2.4Å FWHM) spectroscopy of the Ly α to C IV region was undertaken for all 27 MQS quasars in the range $1.5 < z < 3.0$. To date, observations have been completed for 20/27 of these quasars (see Table 1). Two additional quasars have been observed at Ly α only, namely MRC B0237–233 (a Gigahertz-Peaked Spectrum, GPS, source) and MRC B0246–231 (CSS), and so are not considered in this paper. Of the remaining five quasars, four in the RA range 21h–23h, were missed due to weather-affected observing runs (two lobe-dominated, one core-dominated and one CSS quasar), and MRC B0522–215 (CSS) was not observed on account of its faintness (and its uncertain quasar classification).

The spectroscopy was carried out mostly with the Anglo-Australian Telescope (AAT) at Siding Spring, Australia, and the ESO 3.6m telescope at La Silla, Chile, in several runs between 1995 and 2000. In addition, four faint quasars were observed in 1999 with FORS1 on the VLT UT1 at Paranal, Chile. We note that these observations were challenging due to the faintness of the targets ($19 < b_J < 22$), requiring exposures of several hours each at the highest dispersion with 1200 line/mm gratings, and at least an hour per target in good seeing with 600 line/mm gratings.

Observations at the AAT were carried out in four runs on UT dates 1995 October 19-20, 1996 March 21-22, 1997 February 9-10 and 1999 April 11-12. For the 1995 and 1996 runs we used the RGO spectrograph at f/8 with the 25-cm camera and Tek 1024×1024 CCD and high-dispersion 1200V grating oriented blaze-to-camera. Observations were taken with a 1.5–2″ slit (comparable with seeing) oriented at parallactic angle. The resulting spectral resolution was 1.2Å FWHM. At this dispersion it was necessary to target C IV and/or Ly α (when visible) in separate exposures. Standard star and Cu-Ar comparison lamp spectra were taken at each grating setting. Wavelength calibration is accurate to 0.1Å rms. Conditions were generally not photometric, although the flux densities are reliable to within 30%. All obser-

vations were taken at low airmasses where possible (< 1.2); no extinction corrections were applied.

In the 1997 and 1999 runs, we used the same setup with a 600V grating, giving a spectral resolution of 2.4Å FWHM. Typical seeing for both runs was 1.″2–1.″3, and we used a slit 1.″5 wide, oriented at parallactic angle. Again, wavelength calibration was carried out to within 0.2Å rms with the Cu-Ar lamp spectrum, and spectrophotometric standard stars were observed each night. Conditions were mostly clear for the 1999 run, but cirrus may have affected the 1997 data. No extinction corrections were applied to observations made within 35° of the zenith (i.e. at airmasses smaller than 1.2).

On the ESO 3.6m telescope, EFOSC-2 was used on the nights of 2000 February 1 and 2. The seeing was generally good ($\sim 1''$), and a slit width of 1.″2 was used for the majority of observations (reduced to $1''$ when the seeing was especially good). The slit was placed on the sky at parallactic angle. EFOSC grating #7 was used with a 2048-pixel square detector and 2-pixel binning, to give a mean dispersion of 1.0Å per pixel over the wavelength range 3250–5235Å. Helium-Argon calibration lamp spectra were observed for each object, giving a wavelength accuracy of better than 0.1Å. A spectrophotometric standard star was observed twice nightly. Some objects were observed at large airmasses (1.2–2.0), so extinction corrections were applied after the data were reduced in these cases. The typical exposure time for each quasar was 1 hour.

Observations on the VLT UT1 telescope were made in service-observing mode on 1999 October 17, November 11-13, 15 and December 11-12. The FORS1 instrument was used with a 300B grism, giving a dispersion of 1.2Å per pixel over the wavelength range 3000–7000Å. The slit was $1''$ wide and placed at parallactic angle, and the seeing was always better than $1.2''$. Spectrophotometric standard stars were observed each night. Two-dimensional wavelength solutions were applied to the raw spectral data from archival calibration data. The linearised images were then cleaned of cosmic rays, bias-subtracted and flatfielded before the spectra were extracted. Again the observations were made at low airmasses so extinction corrections were not applied.

All the spectra were reduced using standard procedures in FIGARO, and have been converted to a vacuum-heliocentric wavelength scale.

2.3. HST observations

For direct comparison with the $z \sim 2$ sample, UV spectroscopy was carried out with the STIS instrument on HST for 19 MQS quasars with redshifts $0.7 < z < 1.0$. More precisely, the HST targets comprise all MQS quasars in the redshift range $z = 0.780$–0.950, with the addition of B0123–226 and B1224–262 (with similar redshifts of $z = 0.717$ and 0.77, respectively). MRC B0123–226 was chosen to increase the number of core-dominated quasars (to three) in the HST target list (it has $R = 2.10$, albeit $\alpha = 0.58$, in Table 2), and MRC B1224–262 was added to increase the number of CSS quasars (to four), for statistical reasons. Given the already small number of quasars targetted, both are included in the rest of the analysis (see also Section 5.1). Two sources within the complete redshift-limited sample were not targetted with HST — BL-Lac object B2240–260, and quasar B0418–288 which was too faint ($b_{\rm J} > 21$) to observe with STIS. All targets were detected successfully with STIS, apart from B2156–245, which is both faint ($b_{\rm J} = 20.2$) and red ($\alpha_{\rm opt}= 2$), and is therefore excluded from this analysis.

The HST STIS observations were scheduled at various times between May 1999 and February 2001. The NUV-MAMA detector was used with the G230L grism centred at 2376Å, giving a spectral resolution of 3.0Å over the wavelength range 1570–3180Å. The MAMA detectors have the double advantage of absence of read noise and lack of susceptibility to cosmic rays. A slit of length $52''$ and width 0.″2 was used for the observations. A total of 34 HST orbits was used, with one or two orbits per target depending on its brightness. Exposures in each orbit were split into two, of typical duration 1200s. Standard wavelength and spectrophotometric calibrations were used, and the data were reduced using the standard STIS pipeline. Table 2 details the observations for each target.

3. The spectra

The C IV restframe region is shown for both high- and low-redshift quasars in Figures 1 and 2, respectively. Where more than one ground-based spectrum was taken for the former, only the spectrum with the highest signal-to-noise ratio is shown in Figure 1. Clearly, the C IV profiles shown in the Figures display a wide range of absorption properties.

Absorption systems were identified and measured

in the following way using 'splot' in IRAF for both sets of spectra. Measurements are given in Tables 3 and 4. First, absorption systems were identified in each spectrum lying within $5000\,\mathrm{km\,s^{-1}}$ of the C IV emission-line redshift. The C IV emission-line redshift was measured by fitting a Lorentzian profile to the line wings and using the fitted peak wavelength. Velocities of the narrow absorption lines are defined in the standard way, i.e. $v/c = (A^2-1)/(A^2+1)$ where $A = (1+z_e)/(1+z_a)$ (Foltz et al. 1986), although in practice we approximated this to $\Delta v/c \approx (z_e - z_a)/(1+z_e)$ (for $\Delta v \ll c$). Identification of the C IV absorption lines was confirmed by identifying other lines in the same system, usually including Ly α (see Paper II for identifications of other species), and the ratio of wavelengths of the C IV doublet when it was resolved. In this way we selected the strongest C IV absorption system within $5000\,\mathrm{km\,s^{-1}}$ for further measurement. Velocities were measured using the stronger 1548Å absorption line, or assuming an average wavelength of 1550Å if the doublet was blended. Uncertainties in velocities are dominated by errors in fitting the broad emission-line peaks, which can be uncertain by several Å. Errors are also greater for blended absorption lines. Velocity uncertainties are described more fully in Sections 4.1 and 4.1.1. In four quasars with ground-based spectra, we also noted and measured some weak absorption systems with larger relative velocities, $\Delta v = 5000$–$8000\,\mathrm{km\,s^{-1}}$, but these were ultimately excluded from the main analysis (see Section 4.1).

Equivalent widths ($W_{\rm abs}$) were measured for both lines of the C IV$\lambda\lambda$1548,1550 absorption doublet together, so that blended and unblended lines could be compared. The measurements were made using a simple linear fit across the continuum adjacent to the absorption feature; this was deemed sufficient given the absorption lines are narrow and superposed on the wings of broad emission lines of different shapes. Given the range of emission profiles observed (ranges of widths, 'peakiness', and asymmetries), there is some subjectivity in continuum placement for the equivalent width measurement, particularly when the absorption occurs close to the line peak, in which case the absorption may be underestimated. The $W_{\rm abs}$ measurement errors quoted span the range of reasonable fits to the data by hand, taking continuum-fitting into account, and are typically $\sim 10\%$ for the ground-based observations and ~ 20–30% for the HST observations. The equivalent widths are all quoted in the restframe. Upper limits ($\sim 3\sigma$) to $W_{\rm abs}$ were estimated by eye, corresponding roughly to the largest EW measurable from a noise feature within $5000\,\mathrm{km\,s^{-1}}$ of the emission-line. Thus, they depend on the quality of the individual spectra, the continuum magnitude, and the strength and profile of the C IV emission lines, but are typically $W_{\rm abs} < 0.2$Å for the groundbased and $W_{\rm abs} < 0.3$Å for the HST data (with three noisy HST spectra yielding $W_{\rm abs} < 0.8$Å).

The statistical significance of correlations has been estimated throughout using the Kendall's Tau and Spearman's Rho rank correlation tests as coded in the ASURV program (Isobe & Feigelson 1985, 1986), incorporating upper limits in equivalent widths when relevant. Limits in R and D were not incorporated for the few objects affected due to software limitations, which restrict the application of multiple sets of limits to the data.

3.1. Notes on individual HST spectra

The HST data have lower signal-to-noise ratios and resolution than the ground-based observations, so they are subject to somewhat greater uncertainties in line identification and measurement. Notes are given below for measurements of several quasars, as indicated in Table 4.

B0030–220: the associated C IV absorption system is complex, and is almost certainly blended with Galactic Mg II$\lambda\lambda$2796,2803 at $z \approx 0$. However, the strength of the absorption system, together with the presence of associated Ly α and N V absorption, suggests that associated C IV is primarily responsible. A large, conservative error bar has been assigned to the measured $W_{\rm abs}$ to try to account for the uncertainty due to blended MgII, and the fact that the absorption feature lies close to the emission-line peak.

B0135–247: Galactic Mg II absorption is obvious in the blue wing of the C IV emission line.

B1202–262: Galactic Mg II absorption is visible in the red wing of the C IV emission line.

B1208–277: Both the Ly α and C IV emission lines are narrow, suggesting that the quasar classification of this object is uncertain, and instead it lies on the border-line between a radio galaxy and quasar. The optical spectrum published by Baker et al. (1999) is noisy, but it does not show any strong broad lines and [O II] is weaker than expected in a classical radio galaxy spectrum, consistent with this interpretation.

No absorption is detected against the narrow C IV emission line, but the likelihood of detection is much lower against such narrow lines and weak, noisy continuum. Therefore, given these uncertainties we exclude B1208–277 from the rest of the analysis.

B1349–265: the HST spectrum is very noisy, but strong absorption is clearly seen in Ly α, N V and C IV. There appear to be at least two sets of strong C IV doublets — we have measured only the strongest one here.

B2136–251: the HST spectrum is noisy, but we note that the ratio of N V/Ly α emission is unusually high, and the emission lines are relatively narrow compared with the other quasars observed. Kapahi et al. (1998) classified this quasar as a GPS radio source, and it is the most compact radio source in our sample.

4. Results

4.1. Relative velocities

Figure 3 shows the distributions of velocities relative to the C IV emission-line redshift for all the $z_{\rm a} \approx z_{\rm e}$ absorption systems identified in the ground-based and HST spectra, respectively. In both subsamples the majority (50–70%) of strong absorption systems lies within $500\,{\rm km\,s^{-1}}$ of the emission redshift. At slightly higher relative velocities, between ~ 1000–$3000\,{\rm km\,s^{-1}}$ of the emission redshift, we find both blue- and redshifted systems. There is a slight tendency to find more blueshifted systems, but based on so few objects it is not statistically significant. The means of the velocity distributions of the absorption systems (in Tables 3 and 4) are consistent with no offset from the C IV emission-line redshift ($\langle \Delta v \rangle \approx 40$, $80\,{\rm km\,s^{-1}}$ for the high- and low-redshift datasets, respectively). The standard deviations in the distributions of measured velocities are both $\sim 1000\,{\rm km\,s^{-1}}$ ($\sigma \approx 1300$ and $800\,{\rm km\,s^{-1}}$, respectively; the difference is not significant).

In the ground-based data, where the signal-to-noise ratios are higher, we detected four C IV absorption systems in the emission-line wings with still higher relative velocities, $\Delta v = 5000$–$10000\,{\rm km\,s^{-1}}$ (see Table 3). These are exclusively blue-shifted systems, and all four are seen in core-dominated quasars, as indicated in Figure 4. Possible explanations for seeing such systems only in highly-beamed, core-dominated quasars include (1) geometrical effects, such that we are intercepting faster outflowing gas near the radio-jet axis, or (2) these absorbing clouds arise in foreground galaxies along the quasar sightline. The latter interpretation is consistent with the high-velocity absorption lines being relatively weak ($0.5 < W_{\rm abs} < 1.5$Å) and the lack of any increase in relative velocity with radio core-dominance parameter, R, otherwise in Figure 4. In this case the preferential detection of these high-velocity systems in core-dominated quasars may simply be a selection effect, whereby weak absorption systems will be easier to detect against the brighter continua of highly-beamed quasars, which in addition tend not to show any strong $z_{\rm a} \approx z_{\rm e}$ absorption (see Section 4.3). These four quasars are among the most optically-luminous in our study (only two other quasars have comparable optical luminosities). Similar high-velocity systems in core-dominated quasars have been reported by Richards et al. (1999), and several other examples of quasar ab-

sorbers at extremely high relative velocities are known (e.g. Hamann et al. 1997), but the relationship of this class to either low-velocity or intervening absorbers is unclear at present.

Therefore, we will consider only the class of associated absorption systems with $\Delta v < 5000\,\mathrm{km\,s^{-1}}$ for the rest of this paper. We note that the inclusion of the four weak, high-velocity absorbers would not, in fact, change any of the main conclusions.

4.1.1. Systematic uncertainties in velocity

One uncertainty in the interpretation of relative velocities is that the C IV emission line may not be representative of the systemic redshift of the quasar. It has been noted before that high-ionization lines in quasar spectra, including C IV, may be blueshifted by up to $\sim 1000\,\mathrm{km\,s^{-1}}$ relative to lower ionization and narrow forbidden lines, such as Mg II and [O II]λ3727 (Gaskell 1982; Tytler & Fan 1992; McIntosh et al. 1999). To check whether the velocities measured relative to the C IV emission-line redshift are biased with respect to the systemic redshift of the quasar, we plot in Figure 5 the relative velocities of the absorption systems calculated relative to the C IV and Mg II emission lines, when both were available (Baker et al. 1999; de Silva et al., in preparation). Velocities relative to [O II] are also included for several low-redshift quasars where this line is visible in the optical spectrum. The agreement between the C IV and Mg II redshifts for the ground-based data in Figure 5 is in general good (within $500\,\mathrm{km\,s^{-1}}$), except in two cases (B0328–272 and B2158–206) where C IV is blueshifted relative to Mg II emission by $\sim 1000\,\mathrm{km\,s^{-1}}$. The apparent redshift difference in B2158–206 may, however, be overestimated due to absorption in Mg II (Baker et al. 1999). The scatter for the $z \sim 1$ quasars is somewhat greater, as expected given the lower resolution of the HST data (3Å corresponds to about $300\mathrm{km\,s^{-1}}$ resolution for C IV at 2800Å, and the wavelength calibration for the MAMA detectors themselves is uncertain to within a pixel, or about $150\mathrm{km\,s^{-1}}$) and measurement uncertainties for the emission-line peaks. In fact, the uncertainties in the relative velocities are dominated by the uncertainty in fitting the broad emission-line profile, which is exacerbated by the presence of the absorption itself and also intrinsic profile asymmetries. Thus, uncertainties in Δv relative to the mean C IV emission redshift are $\pm$500–$600\,\mathrm{km\,s^{-1}}$ for both low- and high-redshift datasets, $\pm$700–$800\,\mathrm{km\,s^{-1}}$ with respect to Mg II in the high-redshift subset and as high as $\pm 1000\,\mathrm{km\,s^{-1}}$ for the low-redshift quasars. The higher values for Mg II are due to the lower-resolution of the spectra from which these wavelengths were measured. These uncertainties are seen in the scatter in Figure 5. Thus, apart from the two cases above, there is no strong evidence for a systematic velocity offset between the C IV, Mg II and [O II] emission lines.

Given not all objects have Mg II and/or [O II] emission measurements available, and the effect of a small zeropoint velocity shift is unimportant for the main conclusions of this study, we will continue to refer to velocities relative to the C IV emission-line redshift throughout the rest of the paper.

4.2. Absorption as a function of radio spectral index

Figure 6 shows the equivalent width of the C IV absorption lines as a function of 0.408–5 GHz radio spectral index for both the high- and low-redshift datasets. Strong absorption ($W_{\mathrm{abs}} > 1$Å) is detected *exclusively* in steep-spectrum ($\alpha > 0.5$) quasars in both samples. Statistically, a significant correlation is present, according to both Kendall's Tau and Spearman's Rho rank correlation tests, at the 95% level for the combined datasets. However, looking at the figure, the data seem to define a trend in the upper envelope of the distribution of points, with considerable scatter, rather than a direct linear relationship between the two quantities.

The MQS contains a relatively small number of flat-spectrum quasars due to its low-frequency selection. Nevertheless, the lack of any strong absorption in the six quasars with spectra flatter than 0.5 is marginally significant, i.e. on the null hypothesis, we would otherwise expect about half of them (three) to exhibit strong absorption and none does. Although our study is limited by the small number of flat-spectrum quasars, the prevalence of strong absorbers in steep-spectrum quasars is in good agreement with earlier studies (Anderson et al. 1997; Foltz et al. 1988).

4.3. Absorption as a function of radio-core dominance

The equivalent width of the C IV absorption lines is plotted as a function of radio-core-dominance parameter, R, in Figure 7. CSS quasars are included in a separate panel in Figure 7 for comparison because R-

values were not measurable on account of the small sizes of these sources and the inherent difficulty in identifying core components in them. Together, both the high- and low-redshift samples indicate a trend in Figure 7, such that absorption is greatest in lobe-dominated quasars of low R and decreases steadily with R. The anticorrelation is significant at the 98% level. A similar trend was reported by Barthel et al. (1997) and interpreted in terms of the anisotropic distribution of the absorbers, lying predominantly away from the radio-jet axis.

We note the presence of two apparent outliers in Fig 7, B1355–215 and B0136–231 (labelled Q1 and Q2 on Figure 7, respectively). These both have somewhat uncertain R values by about a factor of two, based on their radio images, and both have steep spectra (see Kapahi et al. 1998). B1355–215 is a small source (35 kpc), only slightly larger than the CSS definition used in this paper. That an occasional absorbing cloud intercepts the line of sight to the quasar even when it is observed close to the jet axis is perhaps not unexpected, especially in smaller sources (see below).

4.4. Absorption as a function of radio-source size

The equivalent widths of C IV absorption are plotted as a function of the projected linear sizes of the radio sources in Figure 8 for both high- and low-redshift datasets. Core-dominated quasars are now excluded as they are severely foreshortened. CSS quasars are included — linear sizes were measured from 1.7-GHz and 5-GHz MERLIN images with typical resolution $0\farcs1$ (de Silva et al. 2001, in preparation). Linear sizes for larger sources are taken from 5-GHz VLA images at $1''$ resolution (see Kapahi et al. 1998). Linear sizes are therefore accurate to better than $\sim 10\%$ in most cases.

It is clear in Figure 8 that the strongest absorption occurs preferentially in the smallest sources. Notably, all but one of the CSS sources show $z_{\rm a} \approx z_{\rm e}$ absorption stronger than $W_{\rm abs} = 1$Å. The exception is MRC B2136–251, a very compact GPS source ($D < 0.2$ kpc) with an unusual UV spectrum (see notes in Section 3.1). The formal probability of an anticorrelation being present is $> 99\%$ for the combined datasets (excluding the GPS source).

Figure 8 demonstrates that, at least in this regard, CSS quasars do not appear to be a class separate from other quasars. Instead, there is a continuous decline in absorption strength as the sources increase in size. Thus, the precise size limit used to define CSS quasars, here 25 kpc (chosen before this absorption-line study was made; see Kapahi et al. 1998), is certainly quite arbitrary, although it corresponds approximately to the typical scale of galaxies (tens of kpc). Nevertheless, it does seem an appropriate limit in that it marks the size below which *all* MQS quasars (apart from GPS source MRC B2136–251) show significant optical absorption. Although the cutoff size is irrelevant in plots such as Figure 8, any comparison of average properties between classes, such as CSS and larger sources, would be diminished in significance proportionately as larger cutoff sizes were used.

In Figure 8, both the high- and low-redshift datasets fall on the same relationship to within a factor of ~ 2. We note that this need not be the case intrinsically, as different cosmological models predict different scaling relationships between observed angular size and projected linear size, and merely the assumption of one set of cosmological parameters rather than another would allow the high- and low-redshift datasets to be moved laterally with respect to each another on Figure 8. Consequently, we can say merely that high- and low- redshift MQS quasars follow the same relationship between absorption strength and linear size for models with angular-size redshift relations similar to the cosmology assumed in this paper. We also note that both high- and low-redshift datasets are indistinguishable in all the other correlations we have presented, which are not cosmology-dependent.

In Figure 9, the velocities of the C IV absorption lines relative to the broad C IV emission redshift are plotted as a function of radio linear size. There is a weak anticorrelation, such that C IV absorption tends to be blueshifted more often in small sources and may be occasionally redshifted in larger sources, but this is highly speculative given the large uncertainties involved (of order $\pm$500–600 km s^{-1} due to measurement) and the statistically small number of quasars with measured absorption. Therefore we merely mention it here, until follow-up observations are made. For comparison, no trend was found between relative velocity and R (Figure 4).

4.5. Reddening by absorbing clouds?

For quasars where C IV absorption was detected, the equivalent width of the absorption is plotted in Figure 10 against the power-law slope of the op-

tical continuum, $\alpha_{\rm opt}$ (as measured between 3500 and 10000Å). There is a remarkably strong correlation (with a probability $> 99\%$) between absorption-line strength and spectral slope — heavily absorbed quasars are systematically redder. The unequivocal correlation argues strongly for a direct relationship between the two, in the sense that C IV absorption implies a redder continuum.

Baker (1997) presented evidence that the range in optical spectral slope observed in the MQS is due in part to reddening by a dust screen lying outside the broad emission-line region. In this earlier study, the most direct evidence for dust reddening (as opposed to intrinsic spectral steepening) was the tight correlation between $\alpha_{\rm opt}$ and the broad-line H α/H β Balmer Decrement, at least in low-redshift ($z < 0.5$) quasars where it was measurable in the optical. By extension, the simplest explanation of the correlation of $W_{\rm abs}$ with $\alpha_{\rm opt}$ in Figure 10 is that the absorbing gas clouds also contain dust, and they lie well outside the nuclear continuum source. In addition, the fact that some quasars without strong C IV absorption have $\alpha_{\rm opt} > 1$ indicates that the dust may have a greater covering fraction than the C IV-absorbing clouds, although absorbed quasars are systematically redder than unabsorbed quasars. Alternatively, if dust is not responsible, then C IV absorption strength correlates with an intrinsically softer continuum shape.

No significant correlations were found between $W_{\rm abs}$ and optical luminosity or magnitude. However, most of the quasars are concentrated in a relatively small range in B-band optical luminosity, $23.5 < \log L_\nu < 24.5$, within the whole range $22.3 < \log L_\nu < 25.2$ (where L_ν is expressed in WHz^{-1}).

5. Discussion

5.1. Orientation and evolution

Evidence was presented in Sections 4.2 and 4.4 that the strongest C IV absorbers are found more often in lobe-dominated, steep-spectrum quasars, but particularly in *small* radio sources. In fact, as Table 5 shows, strong associated absorption ($W_{\rm abs} > 1$Å) was detected in a total of 11/12 ($92 \pm 8\%$) CSS (and GPS) quasars, compared with 8/19 ($42 \pm 11\%$) large steep-spectrum sources ($D > 25$ kpc) and 0/6 flat-spectrum sources (using binomial uncertainties). The median equivalent width of C IV absorption is also correspondingly stronger in CSS quasars than lobe-dominated quasars, and weakest in flat-spectrum sources.

Although the redshift-limited samples are slightly incomplete, the numbers of missing quasars (totalling 5 CSS, 2 lobe-dominated, 1 core-dominated, and 1 GPS quasar) are too small to overturn the above conclusions (and the inclusion of two quasars in the HST sample which are technically outside the redshift-limited subset redresses the balance for lobe-dominated quasars; see Section 2.3). We note that the CSS quasars missed include some of the reddest, and faintest, quasars in the sample, and these very properties are consistent with the thrust of our results. Therefore, we predict that the majority of these unobserved CSS quasars will show strong C IV absorption.

We now discuss whether the above results may be explained by one or a combination of the following hypotheses: (1) the distribution of absorbing clouds is orientation-dependent; (2) absorption strength correlates with the density of the gaseous (or cluster) environment surrounding the quasar; (3) the absorption column density changes with time.

In the orientation-based 'unified schemes' for radio sources, flat-spectrum and core-dominated sources are classified as such because their radio-jet emission is strongly boosted on account of being viewed at a small angle to the axis of the relativistic jet. The cores of more highly-inclined steep-spectrum quasars are less strongly boosted, and so their total radio emission is dominated by the isotropically emitted radiation from their diffuse lobes. Thus, in these models the prevalence of absorption in steep- rather than flat-spectrum sources, and its decrease with R, would imply that the absorbing material lies preferentially away from the jet axis, increasing in column density the greater the inclination angle. Similar results were interpreted this way in earlier studies (Anderson et al. 1987; Foltz et al. 1988; Barthel et al. 1997; Richards et al. 1999, 2001). The merits of the unified schemes themselves are argued at length elsewhere (see reviews by Antonucci 1993; Padovani & Urry 1995). However, orientation alone cannot explain the range of sizes of steep-spectrum quasars, including CSS quasars, so another process is required to explain the decrease in C IV absorption column density with increasing radio size.

If the absorbing material arises in dense quasar environments then we would expect to see its signature clearly either in studies of the host galaxies or the cluster environments of quasars. If this

were the case, steep-spectrum and small sources (CSS quasars) should inhabit more dense, gas-rich environments than flat-spectrum and larger sources, respectively. However, there is currently no observational evidence to support this simple view (O'Dea 1998; Wold et al. 2000; Saikia et al. 2001). Instead, it seems that quasars of all types are found in environments spanning a wide variety of richness (Yee & Green 1987; Gelderman 1996; Wold et al. 2000; Palma et al. 2000), from average field density to poor groups to rich clusters. In this respect the MQS appears to be no different, as has been demonstrated in preliminary imaging of MQS fields with $0.7 < z < 1.0$ (Bremer & Baker 1999; Baker et al. 2001; Bremer, Baker & Lehnert 2001). Although the dispersion in relative velocities of the C IV absorption systems ($\sigma \sim 1000$ km s^{-1}) is comparable with that of galaxies in massive clusters (e.g. Postman, Lubin & Oke 2001), such clusters should be rare at $z > 1$ (e.g. Bahcall & Fan 1998; Bode et al. 2001), and so it is unlikely that a trend such as that seen in Figure 8 would be generated by random cluster galaxies intercepting the line of sight to the quasar. The host galaxies of all classes of radio-loud AGN (radio galaxies, quasars and CSS sources) also appear to be virtually indistinguishable in terms of mass, size and colour (Heckman et al. 1994; Hes, Barthel & Hoekstra 1995; Fanti et al. 2000; de Vries et al. 2000) once the effect of beamed emission in quasars is taken into account. However, there is evidence that some CSS sources are brighter in the far infrared, as a consequence of enhanced starburst activity and/or high dust content (Hes, Barthel & Hoekstra 1995).

Theoretically, arguments for the pressure confinement of radio lobes imply environmental density must affect source size to some extent (e.g. Barthel & Arnaud 1996). Asymmetric sources provide a clear illustration — the shorter lobe tends to be associated with higher galaxy densities (Bremer et al. 2001; Barr, Bremer, Baker 2001), higher radio depolarisation (Garrington et al. 1988; Garrington & Conway 1991; Ishwara-Chandra et al. 1998) and radio fluxes, and brighter extended line emission (McCarthy, van Breugel & Kapahi 1991), all of which are indicative of higher densities on the shorter-lobe side. Typical length ratios of lobes in asymmetric sources are about 2–3 or smaller, indicative of density contrasts of up to an order of magnitude between the two sides. However, to constrict sources to scales of tens rather than hundreds of kpc would require overdensities of several orders of magnitude, which is not seen at any other wavelength. There is evidence that some CSSs do inhabit moderately gas-rich environments, mostly through radio polarisation and H I 21-cm absorption measurements on sub-kpc scales (Akujor & Garrington 1995; van Gorkom et al. 1989; Conway 1996; Peck et al. 1999, 2000; Vermeulen 2001), but it is not clear whether these environments are exceptional. There is also no evidence that CSS jets are slowed appreciably, as their hotspot advance speeds appear normal ($v \sim 0.2c$) (Taylor et al. 2000). Thus most CSS jets are unlikely to be confined permanently by ultradense gas, but the range of environments that quasars inhabit must introduce variations of factors of up to a few in absolute size. Other factors, such as jet power, will also introduce scatter (de Silva et al., in preparation). Some CSS sources might also be short-lived.

If environmental density alone cannot account for the full range of source sizes, then age must be important. To explain the results of this paper, the absorption column density must decrease over the lifetime of an expanding radio source. Recent radio VLBI observations (Readhead et al. 1996; Taylor et al. 2000; Peck et al. 2000) and spectral shape analyses (Murgia et al. 1999; Snellen et al. 2000) do indeed infer ages as young as 10^2–10^4 years for CSS sources compared with the canonical 10^7–10^8 years for larger radio sources. Processes which might clear the absorbing material are discussed below.

5.2. Dust in the absorbing clouds

As well as the strong dependence on radio properties, Section 4.5 suggests that the absorbers contain dust, which systematically reddens the continuum. The strong correlation between absorption strength and continuum slope in Figure 10 suggests, somewhat surprisingly, that the dust and highly-ionised gas exist in close proximity, perhaps even in the same clouds.

The fact that reddening is occurring at all indicates the presence of small dust grains in the quasar emission-line regions. Such grains should be destroyed easily by sputtering by hot gas (Ferrara et al. 1991), shocks (Jones, Tielens & Hollenbach 1996), collisions and evaporation. De Young (1998) assessed in detail the problem of survivability of dust grains in the vicinity of powerful radio galaxies, where strong shocks and hard radiation are undoubtedly present, and found that under most circumstances 100–2500Å graphite grains should be completely destroyed within 10^4–10^6 years. Special conditions are required for

grain survival up to $\sim 10^7$ years, namely low shock velocities and dense clouds, or alternatively (but more unlikely) a hot, rarefied medium. Otherwise, dust replenishment is necessary. Dust may be created by new and extensive star formation, entrained from ISM clouds or torus material by turbulent flows within the radio cocoon, or redistributed by galactic winds. Thus, over the lifetime of a radio source, dust grains will be created and destroyed by many processes and over many astrophysical cycles. Yet, the net outcome of the dust recycling is gradual clearing, at least along the radio axis. With respect to models for the emergence of quasars from their dusty cocoons, we can set an approximate timescale of $\sim 10^{5-6}$ years, comparable with the lifetime of CSS sources, for the ionisation cones to be opened up significantly.

Because the absorption lines in our dataset are strong and mostly saturated, we cannot measure accurate gas column densities from a simple curve-of-growth analysis. The lack of damping wings in Ly α puts a rough upper limit at $N_{\rm HI} < 10^{20}\,{\rm cm}^{-2}$ for neutral gas in the optical absorber, although the hydrogen is likely to be highly ionised in the C IV-absorbing regions so the total gas mass will be higher. To produce reddening of $E_{\rm B-V} = 0.3$–1.0, the range applicable to MQS quasars (see also Baker 1997), would require a dust-to-gas ratio comparable with or greater than the Galactic value. For example, if we assume the mean Galactic ratio of $\langle N_{\rm HI}/E_{\rm B-V}\rangle = 5.2 \times 10^{21}$ ${\rm cm}^{-2}$ ${\rm mag}^{-1}$ (Shull & van Steenberg 1985), then we would need $N_{\rm HI} \sim 10^{21}\,{\rm cm}^{-2}$ to produce $E_{\rm B-V} =$ 0.3–1.0. Although a more detailed quantitative analysis is required, this indicates that the dust content of the absorbers is relatively high.

A decline similar to that shown in Figure 10 of $W_{\rm abs}$C IV with increasing UV spectral slope has been recently reported by Vestergaard (2001) for a mixed radio-loud and -quiet sample, suggesting that the absorbers in radio-quiet quasars also contain dust. If these results can indeed be extended to all quasars, an immediate consequence of the presence of dust in the associated absorbers is that absorbed quasars will tend to be missed preferentially in optically-selected samples, especially those selected in the blue and ultraviolet. This may help explain the paucity of associated absorbers in such samples (e.g. only 10% of LBQS quasars show associated absorption, Weymann et al. 1991; Ganguly et al. 2001). Radio-quiet quasars are discussed further in Section 5.5. As a precedent, Fall & Pei (1993) showed that intervening damped Ly α absorbers also redden the light from background quasars, resulting in a systematic loss of reddened sightlines from quasar absorption-line studies. Therefore, we would expect that even larger numbers of AGN will be reddened and dimmed by *their own* dusty halos.

We note that the fraction of CSS sources among MRC 1-Jy quasars and radio galaxies is approximately the same, $\sim$ 23% (Kapahi et al. 1998). This implies that the inner torus opening angle is not significantly different for small and large sources (Saikia et al. 2001), but the broad lines in smaller sources are generally more reddened by dust at radii outside the broad-line region. We note a class of CSS sources which are borderline quasars/radio galaxies (e.g. MRC B1208–277 and two similar objects with spectra shown in Baker et al. 1999) where the broad lines are weak or non-existent but the narrow emission lines have higher excitation than expected for normal radio galaxies. These may be highly reddened CSS quasars, but their numbers are too small to significantly affect the quasar fraction in the MRC 1-Jy sample.

5.3. Redshift

We note that the results of this paper are all independent of redshift, i.e. in a flux-limited sample we found no marked differences between the global properties or frequency of C IV associated absorption in quasars at $0.7 < z < 1.0$ and $1.5 < z < 3.0$. This is contrary to the proposition of Ganguly et al. (2001) that strong $z_{\rm a} \approx z_{\rm e}$ absorption systems are rarer at $z < 1.2$ than at $1.4 < z < 2.0$. Ganguly et al. (2001) found associated absorption systems with $W_{\rm abs} > 1.5$Å in only 1/13 steep-spectrum quasars with $z < 1.2$ drawn from the UV-bright sample of the HST Absorption-Line Key Project, compared with 8/24 steep-spectrum quasars with $1.4 < z < 2.0$ from the sample of Foltz et al. (1986). The latter fraction, $\sim$ 30%, is in good agreement with the number of absorption systems with $W_{\rm abs} > 1.5$Å in both our HST (5/17) and ground-based (8/20) datasets. In addition, the finding that C IV absorbers are just as common at $z \sim 0.8$ as at $z \sim 2$ may have implications for the interpretation of associated Ly α absorbers in high-redshift radio galaxies (Barthel & Miley 1988; Röttgering et al. 1995; van Ojik et al. 1997; De Breuck et al. 2000). Interestingly, the associated absorption in high-redshift radio galaxies is found to be most common in sources less than 50 kpc in size, rais-

ing the idea that some high-redshift radio galaxies are essentially similar to CSS quasars.

Redshift-independence indicates that the absorbing material arises in structures which are not evolving significantly with cosmic time. This point argues against many galactic origins for the absorbing clouds, for example in surrounding clusters, star-forming and dwarf galaxies, which should show strong evolution between these epochs. There remain two plausible explanations: either the material is linked directly to processes within the active nucleus, or we see the absorbers only as a transient property of a galaxy system viewed at one particular stage in its evolution. In the latter case, the phase must be seen commonly alongside the AGN phenomenon, even if it is not intrinsic to it.

Processes intrinsic to the AGN include winds or outflows from the quasar nucleus, which should be governed by basic properties of the AGN central engine (black-hole mass, spin, fuelling rate). Otherwise, the absorbers might mark a unique environment or jet-triggering event, which is essential for the formation of radio jets. For example, mergers between massive galaxies might produce similar outcomes, irrespective of redshift.

Alternatively, competing effects (quasar luminosity, redshift) might somehow have contrived to cancel out evolutionary trends in our flux-limited sample. The ranges of radio power at 408 MHz (expressed in $\mathrm{W\,Hz^{-1}}$) sampled for the low- and high-redshift MQS samples are $27.3 < \log P_{408} < 28.2$ (median $\log P_{408} = 27.7$) and $28.1 < \log P_{408} < 29.0$ (median $\log P_{408} = 28.5$), respectively (Kapahi et al. 1998). So, the high-redshift sample is about a factor of 6 more luminous in the radio on average. In terms of optical B-band luminosity, the difference is less pronounced and the scatter greater, presumably because of the effects of dust. B-band optical luminosities (again expressed in $\mathrm{W\,Hz^{-1}}$) span $22.3 < \log L_\nu < 24.6$ (median $\log L_\nu = 23.7$) and $23.6 < \log L_\nu < 25.2$ (median $\log L_\nu = 24.1$) for the low- and high-redshift quasar samples, respectively. Measurements of larger numbers of absorbers over a wider range in redshift and luminosity would be needed to distinguish between these scenarios.

5.4. Origin of absorbing clouds

The most fundamental question remains the origin of the absorbing gas. Where distances to the clouds can be estimated from excited-state fine-structure absorption lines (which necessarily require the presence of dense clouds far from the nuclear radiation) they are large — of order tens of kpc (Hamann et al. 2001). This would put the clouds in or near the extended narrow emission-line regions of quasars, where we already see large quantities of ionised gas (Lehnert et al. 1992, Bremer et al. 1992) and dust (Andreani, Franceschini, Granato 1999; Polletta et al. 2000; Haas et al. 2000; Vernet et al. 2001).

Typical line widths measured for extended (narrow) emission-lines are of order $1000\,\mathrm{km\,s^{-1}}$ (Lehnert & Becker 1998; Heckman et al. 1991; van Oijk et al. 1997; Baum & McCarthy 2000), which is comparable with the range of absorption velocities seen here, and suggests that the gas is turbulent. The origin of the large velocities is uncertain, as it is difficult to disentangle the effects due to the radio jet from those arising simply in the surrounding potential well (van Oijk et al. 1997; Baum & McCarthy 2000). Direct interactions between the radio jet and Ly α clouds have also been noted (Barthel & Miley 1988; van Ojik et al. 1997; Lehnert et al. 1999). In several high-redshift radio galaxies Ly α absorption has been resolved spatially out to $\sim 100\,\mathrm{kpc}$, where it is strongest in radio galaxies with sizes less than 50 kpc and knotty radio structures (Barthel & Miley 1988; Röttgering et al. 1995; van Ojik et al. 1997; De Breuck et al. 2000). Absorption by dense H I gas on compact scales is also seen in radio observations towards many quasars (Vermeulen 2001; Morganti et al. 2001), especially compact sources. Although the amount and location of the H I gas are still being assessed, it may be anisotropic (Morganti et al. 2001) and jet-cloud interactions have been noted in a number of cases (Oosterloo et al. 2000). Absorbing gas with equivalent $N_\mathrm{H} \sim 10^{21-24}\,\mathrm{cm^{-2}}$ has also been inferred from soft X-ray absorption seen towards many quasars (Elvis et al. 1994; Reynolds 1997; Gallagher et al. 2001). Thus, the extended emission-line regions of quasars are known to contain enough gaseous material to account for the C IV absorption and its kinematics, although the exact location of the absorbing clouds is still an open question.

As to its origin, dusty, metal-enriched clouds of H I gas could conceivably be relics of a merger with a gas-rich galaxy, and remnants of star-formation triggered by the merger. However, mergers are efficient only at low relative velocities, so they would predict very low velocity dispersions for the absorbing ma-

terial, contrary to observations. Alternatively, cooling flows might be responsible for depositing the gas (Bremer, Fabian & Crawford 1997; Nulsen & Fabian 2000), although quasars are not necessarily in rich clusters, and the large dust content may be difficult to achieve in a cooling flow model. Some AGN halos have kinematics which are inconsistent with either scenario (Shopbell, Veilleux & Bland-Hawthorn 1999). Otherwise, the gas may simply arise in the potential wells of gas-rich galaxy groups and clusters, or protoclusters, a suggestion supported by the discovery of companion star-forming galaxies around some high-redshift radio galaxies and quasars (Bremer, Fabian & Crawford 1997; Pentericci et al. 2000; Ivison et al. 2000; Baum & McCarthy 2000).

An alternative hypothesis is that the absorbing clouds are embedded in or ejected by nuclear outflows or galactic winds. Interestingly, Heckman et al. (2000) have reported a correlation analogous to Figure 10 in observations of starburst galaxies, namely between the spectral slope of the UV continuum and the equivalent width of Na D absorption from the dusty superwind. Starburst superwinds typically cover a much smaller range of velocities than seen in quasar absorbers, but it is interesting to ask whether the quasar absorbers represent an extreme case of the galactic wind phenomenon. Chen, Lanzetta & Webb (2001) propose that $\sim 100\,$kpc C IV-absorbing halos may be common around even normal galaxies, presumably enriched by galactic wind activity. Radio H I measurements and sensitive optical narrow-band imaging will be crucial for disentangling the origins of the gas.

The results of this paper provide additional clues to the origin of the absorbing clouds. The anticorrelation of absorption strength with source size, if it can be interpreted in terms of age, implies that radio jets are triggered in an environment rich in gas and dust. Mergers have long been thought likely causes of AGN activity, as they will efficiently funnel gas onto the galaxy nucleus. In addition, major mergers are expected to cause massive starbursts, providing a natural explanation for the origin of the dusty material. Thus, starbursts may have a symbiotic relationship with AGN, (González-Delgado, Heckman & Leitherer 2001; Barthel 2001; Canalizo & Stockton 2000). A similar picture has been put forward by Sanders et al. (1988) where ultra-luminous infrared galaxies are proposed as the dusty progenitors of optical quasars. However, in the radio-loud case we have been able to demonstrate a natural age sequence. We discuss this further in Section 5.6.

Another alternative is that the absorbers originate in AGN-driven nuclear outflows (Elvis 2000; de Kool 1997; Proga, Stone & Kallman 2000). However, in these models the decrease in absorbing column density with radio size may be difficult to explain. The main mechanism to decrease the outflow rate is to steadily decrease the accretion rate of material onto the black hole, but this should have other observable repercussions such as dimming the nuclear light and reducing the jet power in large sources.

5.5. Relationship with radio-quiet quasars

The results reported here raise further questions about the apparent differences between radio-loud and radio-quiet quasars. It is widely held that radio-quiet quasars have a lower incidence of associated absorption than radio-loud quasars. The fraction of radio-quiet quasars with $z_{\rm a} \approx z_{\rm e}$ absorption ranges from $\sim$ 10–15% (Foltz et al. 1988; Weymann et al. 1991; Ganguly et al. 2001) to $\sim$ 30% (Vestergaard 2001), compared with 40–50% of radio-loud quasars in low-frequency selected samples, including the MQS. Although these numbers clearly show that consensus has not yet been reached, it has been found that narrow associated-absorption systems are more common amongst certain types of radio-quiet quasars, notably soft-X-ray weak quasars (Brandt, Laor & Wills 2000; Ganguly et al. 2001) and perhaps low-luminosity quasars (Møller & Jakobsen 1987; but see Foltz et al. 1988; and mixed results in Vestergaard 2001). Therefore, it seems likely that sample selection criteria will affect the frequency of finding $z_{\rm a} \approx z_{\rm e}$ systems, although it remains to be seen how severely.

If both radio-loud and radio-quiet quasars have a similar distribution of absorbing material then the brightest optically-selected quasars should be viewed preferentially along clear sightlines to the nucleus within $\sim 20^\circ$–30° of some polar axis, avoiding most of the obscuring material. The presence of dust in the off-axis material would accentuate this natural bias further. Therefore, we would expect to find more associated absorption systems in samples that include fainter, redder quasars. If the hypothesis that both classes are similar is true, then we might predict that the proportion of radio-quiet quasars showing absorption will ultimately rise to match that of the radio-loud quasars. Otherwise, the distributions of dust and gas must differ. The recent preliminary results of

Vestergaard (2001) indeed point to gross similarities between the global reddening and absorption properties of radio-quiet and radio-loud quasars, despite the difficulties inherent in matching samples across these two classes. In addition, Crenshaw et al. (1999) have found a significantly higher rate of occurrence of narrow associated-absorption systems in Seyfert 1 galaxies than was first appreciated, a fraction of $\sim 50\%$ comparable with the radio quasars in this paper. We note that the classification of AGN as either radio-loud or -quiet is especially difficult for AGN of moderate radio luminosity, including Seyfert galaxies, where the radio and optical emission may be contaminated by starburst activity, emission from the host galaxy and relativistic boosting (e.g. Miller, Rawlings & Saunders 1993; Falcke, Sherwood & Patnaik 1996; Ho & Peng 2001; and see Blundell & Rawlings 2001).

In the far-infrared, the distribution of dust in radio-loud and radio-quiet quasars is still under investigation. Both classes have similar far-infrared properties (Andreani et al. 1999; Haas et al. 2000; Polletta et al. 2000), suggesting they harbour comparable amounts of cool dust, characteristic of dusty ISM warmed by star-formation. More work is needed, however, to investigate warmer dust components in the two classes, where emission reprocessed by the circumnuclear torus dominates.

If the covering factor of the absorbing clouds declines with age, then many young, dust-enshrouded AGN will be missing from optically-selected samples. The precise number would depend on the timescale for clearing the material. Based on the assumption that ultra-luminous infrared galaxies (ULIRGs) evolve into quasars (e.g. Sanders et al. 1988), Canalizo & Stockton (2001) estimate that it takes $\sim 50\,\mathrm{Myr}$ for a radio-quiet quasar to emerge from its ULIRG phase. This timescale is longer than the CSS lifetime ($< 1\,\mathrm{Myr}$) discussed in Section 5.1, suggesting that dust is dissipated faster in quasars with radio jets.

In optically-selected quasars, Brandt et al. (2000) reported a strong correlation between $W_{\mathrm{abs}}(\mathrm{C\ IV})$ and the optical to X-ray slope, α_{ox}, linking C IV and soft X-ray absorption. We are not able to see a similar correlation in our sample for the few quasars we have detected in the ROSAT All Sky Survey (Baker, Hunstead & Brinkmann 1995), but this is not surprising given the large number of non-detections. However, Baker et al. (1995) did note that CSS quasars as a group were detected much less often in the RASS, which may indicate X-ray absorption or intrinsic weakness (see also O'Dea 1998). Obviously more X-ray data are needed for the MQS.

As for broad absorption lines (BALs), which favour radio-quiet quasars and originate much closer to the AGN, it is still an open question why they are seen so rarely in radio-loud objects. We note that there is now considerable evidence for dust in BAL systems (Sprayberry & Foltz 1992; Turnshek et al. 1994; Egami et al. 1996; Brotherton et al. 1998).

5.6. Consistent overall picture

Given the redshift-independence and clearing of absorbing material with time, and especially the evidence that radio activity can be recurrent, the presence of dusty absorbing gas *must* be intimately related to the onset of the radio activity, rather than just the host galaxy or cosmic time. Such a build-up of dusty material would occur naturally following a large burst of star-formation, either during or following a merger with a gas-rich galaxy.

Over the source's lifetime, the enshrouding material is gradually cleared, primarily along the jet axis. The bow-shock of the radio source will be particularly efficient in compressing and heating the clouds and shattering dust grains as it passes. The absence of any absorption close to the jet axis itself (in core-dominated, flat-spectrum quasars) suggests that the direct interaction of the radio beam on the ISM clouds may be particularly effective in shocking and displacing material near the hotspot region, punching a hole in the enshrouding gas. Away from the jet, substantial replenishment of dust is likely to occur by, for example, turbulent entrainment at the edges of the cocoon, evaporation from the torus, extended star-formation or galactic winds. Dust may be deposited in disks, or fed back into the torus. Thus the torus must comprise recycled ISM material, and vice versa. Turbulence inside the lobe cavity may also shred clouds, exposing the large surface area to ionizing radiation and producing aligned optical emission with high velocity dispersion (Bremer et al. 1997; Best, Longair & Röttgering 1996).

The basic test for this picture is that CSS sources should show more evidence of recent star-formation than larger sources. There is so far mixed evidence that CSS quasars are brighter in the far-infrared (Hes et al. 1995). On a more detailed level, one might compare the estimated ages of starburst knots and the ra-

dio source. At least in one case, the CSS quasar 3C48 (Canalizo & Stockton 2000), the ages are found to be consistent. Extending this technique to higher redshifts, however, is more difficult. Estimating ages for radio sources is also a fine art; a new practical method applied to the present sample will be presented by de Silva et al. (2001, in preparation).

Finally, we note that apart from the merger/starburst hypothesis, the only plausible alternative is that an AGN-driven wind model might be contrived in which the mass flow declines markedly 10^5 years after the onset of radio activity.

6. Conclusions

We present a study of C IV associated absorption in a highly-complete, homogeneous sample of radio-loud quasars. The main results are:

- We confirm that absorption is more common in steep-spectrum and lobe-dominated quasars, such that the absorbing material lies away from the jet axis in the orientation-dependent unified models.
- The strength of C IV absorption decreases with increasing radio-source size. If we assume that the larger sources are older than the smaller (CSS) ones, then we can attribute the decrease in column density to the growth of the radio-source envelope through the ISM of the host galaxy.
- From the correlation of C IV absorption strength with optical spectral slope, we conclude that considerable amounts of dust are associated with the absorbing clouds. Consequently we predict that absorbed quasars will be missed preferentially in optically-selected samples, provided similar schemes apply.
- We find no evidence for changes in the frequency or strength of the absorbers with redshift from $z \sim 0.7$ to $z \sim 3$. This lack of cosmic evolution indicates the absorbers are unaffected by gross galaxy evolution, rather they signal a transient phase which is related specifically to the AGN activity.
- The combination of these results requires that radio sources are triggered in gas-rich, dusty galaxies, such as those immediately following a starburst, and the dust and gas dissipates over the lifetime of the radio source. Thus, the ionization cones may open up with increasing radio-source age.

The referee is thanked for a detailed reading of the manuscript and useful comments. We thank the staff at the Anglo-Australian Telescope and at ESO, La Silla and the VLT for their help during observing runs. We also thank Tara Murphy for her work on the HST data. JCB acknowledges support which was provided by NASA through Hubble Fellowship grant #HF-01103.01-98A from the Space Telescope Science Institute, which is operated by the Association of Universities for Research in Astronomy, Inc., under NASA contract NAS5-26555, and also PPARC. RWH acknowledges funding from the Australian Research Council.

REFERENCES

Akujor C.E., Garrington S.T., 1995, A&AS, 112, 235

Anderson S.F., Weymann R.J., Foltz C.B., Chaffee F.H. Jr, 1987, AJ, 94, 278

Andreani P., Franceschini, A., Granato G., 1999, MNRAS, 306, 161

Antonucci R., 1993, ARA&A, 31, 473

Bahcall N., Fan X., 1998, ApJ, 497, 188

Baker J.C., 1997, MNRAS, 286, 23

Baker J.C., Hunstead R.W., 1995, ApJL, 452, L95

Baker J.C., Hunstead R.W., Brinkmann, W., 1995, MNRAS, 277, 553

Baker J.C., Hunstead R.W., Kapahi V.K., Subrahmanya C.R., 1999, ApJS, 122, 29

Baker J.C., Hunstead R.W., Bremer M.N., Bland-Hawthorn J., Athreya R.M., Barr J., 2001, AJ, 121, 1821

Barr J.M., Bremer M.N., Baker J.C., 2001, in 'QSO Environments', ed. I. Marquez (Dordrecht: Kluwer) in press (astroph/0104310)

Barthel P.D., Miley G.K., 1988, Nature, 333, 319

Barthel P.D., 1989, ApJ, 336, 606

Barthel P.D., Arnaud K.A., 1996, MNRAS, 283, L45

Barthel P.D., Tytler D., Vestergaard M., 1997, in ASP Conf. Ser. 128, 'Mass ejection from AGN', eds. N. Arav, I. Shlosman, R.J. Weymann (San Francisco: ASP), 48

Barthel P.D., 2001, in 'The far-infrared and submillimeter energy distributions of active and starburst galaxies', eds. I. van Bemmel, P. Barthel, B. Wilkes, New Astronomy Reviews, 45, 591

Baum S.A., McCarthy P.J., 2000, AJ, 119, 2634

Becker R.H., Gregg M.D., Hook I.M., McMahon R.G., White R.L., Helfand D.J., 1997, ApJ, 479, L93

Becker R.H., White R.L., Gregg M.D., Brotherton M.S., Muehleisen S.A., Arav N., 2000, ApJ, 538, 72

Best P.N., Longair M.S., Röttgering H.J.A., 1996, MNRAS, 280, L9

Blundell K.M., Rawlings S., 2001, ApJL, 562, 5

Bode P., Bahcall N.A., Ford E.B., Ostriker J.P., 2001, ApJ, 551, 15

Brandt, W.N., Laor A., Wills B.J., 2000, ApJ, 528, 637

Bremer M.N., Crawford C.S., Fabian A.C., Johnstone R.M., 1992, MNRAS, 254, 614

Bremer M.N., Fabian A.C., Crawford C.S., 1997, MNRAS, 284, 213

Bremer M.N., Baker J.C., 1999, in 'The Most Distant Radio Galaxies', eds H.J.A. Röttgering, P.N. Best, M.D. Lehnert, p425

Bremer M.N., Baker J.C., Lehnert M., 2001, MNRAS, submitted

Brotherton M.S., van Breugel W., Smith R.J., Boyle B.J., Shanks T., Croom S.M., Miller L., Becker R.H., 1998, ApJL, 505, 7

Canalizo G., Stockton A., 2000, ApJ, 528, 201

Canalizo G., Stockton A., 2001, ApJ, 555, 719

Chen H.-W., Lanzetta K.M., Webb J.K., 2001, ApJ, 556, 158

Conway J. 1996, Procs Leiden CSS/GPS Workshop, eds Snellen et al. (Leiden University), 198

Crenshaw D.M., Kraemer S.B., Boggess A., Maran S.P., Mushotzky R.F., Wu C.-C., 1999, ApJ, 516, 750

De Breuck C., Röttgering H., Miley G., van Breugel W., Best P., 2000, A&A, 362, 519

de Kool M., 1997, in ASP Conf. Ser. 128, 'Mass ejection from AGN', eds. N. Arav, I. Shlosman, R.J. Weymann (San Francisco: ASP), 233

de Vries W.H., O'Dea C.P., Barthel P.D., Fanti C., Fanti R., Lehnert M.D., 2000, AJ, 120, 2300

De Young, D.S., 1998, ApJ, 507, 161

Egami E., Iwamuro F., Maihara T., Oya S., Cowie L.L., 1996, AJ, 112, 73

Elvis M., Fiore F., Mathur S., Wilkes B.J., 1994, ApJ, 425, 103

Elvis M., 2000, ApJ, 545, 63

Falcke H., Sherwood W., Patnaik A.R., 1996, ApJ, 471, 106

Fall, M., Pei Y., 1993, ApJ, 402, 479

Fanti C. et al., 2000, A&A, 358, 499

Fanti R. et al., 1990, A&A, 231, 333

Ferrara A., Ferrini F., Barsella B., Franco J., 1991, ApJ, 381, 137

Foltz C.B., Weymann R.J., Peterson B.M., Sun L., Malkan M.A., Chaffee F.H. Jr, 1986, ApJ, 307, 504

Foltz C.B., Chaffee F.H. ,Weymann R.J., Anderson, S.F., 1988, in 'QSO absorption lines: Probing the Universe', eds. J.C. Blades, D.A. Turnshek, C.A. Norman (Cambridge: CUP), 53

Gallagher S.C., Brandt W.N., Laor A., Elvis M., Mathur S., Wills B.J., Iyomoto N., 2001, ApJ, 546, 795

Ganguly R., Bond N.A., Charlton J.C., Eracleous M., Brandt W.N., Churchill C.W., 2001, ApJ, 549, 133

Garrington S.T., Leahy J.P., Conway R.G., Laing R.A., 1988, Nature, 331, 147

Garrington S.T., Conway R.G., 1991, MNRAS, 250, 198

Gaskell C.M., 1982, ApJ, 263, 79

Gelderman R., Whittle M., 1994, ApJS, 91, 491

Gelderman R., 1996, in Procs Leiden CSS/GPS Workshop, eds Snellen et al. (Leiden University), 208

González-Delgado R.M., Heckman T., Leitherer C., 2001, ApJ, 546, 845

Gregg M.D., Becker R.H., Brotherton M.S., Laurent-Muehleisen S.A., Lacy M., White R.L., 2000, ApJ, 544, 142

Haas M., Müller S.A.H., Chini R., Meisenheimer K., Klaas U., Lemke D., Kreysa E., Camenzind M., 2000, A&A, 354, 453

Hamann F., Barlow T., Cohen R.D., Junkkarinen V., Burbidge E.M., 1997, in ASP Conf. Ser. 128, 'Mass ejection from AGN', eds. N. Arav, I. Shlosman, R.J. Weymann (San Francisco: ASP), 19

Hamann F., Ferland G., 1999, ARA&A, 37, 487

Hamann F.W., Barlow T.A., Chaffee F.C., Foltz C.B., Weymann R.J., 2001, ApJ, 550, 142

Heckman T.M., Miley G.K., Lehnert M.D., van Breugel W., 1991, ApJ, 370, 78

Heckman T.M., O'Dea C.P., Baum S.A., Laurikainen E., 1994, ApJ, 428, 65

Heckman T.M., Lehnert M.D., Strickland D.K., Armus L., 2000, ApJS, 129, 493

Hes R., Barthel P.D., Hoekstra H., 1995, A&A, 303, 8

Ho L.C., Peng C.Y., 2001, ApJ, 555, 650

Ishwara-Chandra C.H., Saikia D.J., Kapahi V.K., McCarthy P.J., 1998, MNRAS, 300, 269

Isobe T., Feigelson E., 1985, ApJ, 293, 192

Isobe T., Feigelson E., 1986, ApJ, 306, 490

Ivison R.J., Dunlop J.S., Smail I., Dey A., Liu M.C., Graham J.R., 2000, ApJ, 542, 27

Jones A.P., Tielens A.G.G.M., Hollenbach D.J., 1996, ApJ, 469, 740

Kapahi V.K., Athreya R.M., Subrahmanya C.R., Baker J.C., Hunstead R.W., McCarthy P.J., van Breugel W., 1998, ApJS, 118, 327

Large M.I., Mills B.Y., Little A.G., Crawford D.F., Sutton J.M., 1981, MNRAS, 194, 693

Lehnert M.D., Heckman T.M., Chamber K.C., Miley G.K., 1992, ApJ, 393, 68

Lehnert M.D., Becker R.H., 1998, A&A, 332, 514

Lehnert M.D., van Breugel W.J.M., Heckman T.M., Miley G.K., 1999, ApJS, 124, 11

McCarthy P.J., van Breugel W.J.M., Kapahi V.K., 1991, ApJ, 371, 478

McIntosh D.H., Rix H.-W., Rieke M.J., Foltz C.B., 1999, ApJL, 517, 73

Miller P., Rawlings S., Saunders R., 1993, MNRAS, 263, 425

Møller P., Jakobsen P., 1987, ApJL, 320, 75

Morganti R., Oosterloo T.A., Tadhunter C.N., van Moorsel G., Killeen N., Wills K.A., 2001, MNRAS, 323, 331

Murgia M., Fanti C., Fanti R., Gregorini L., Klein U., Mack K.-H., Vigotti M., 1999, A&A, 345, 769

Nulsen P.E.J., Fabian A.C., 2000, MNRAS, 311, 346

O'Dea C.P., 1998, PASP, 110, 4930

Oosterloo T.A., Morganti R., Tzioumis A., Reynolds J., King E., McCulloch P., Tsvetanov Z., 2000, AJ, 119, 2085

Owsianik I., Conway J.E., 1998, A&A, 337, 690

Palma C., Bauer F.E., Cotton W.D., Bridle A.H., Majewski S.R., Sarazin C.L., 2000, AJ, 119, 2068

Peck A.B., Taylor G.B., Conway. J.E., 1999, ApJ, 521, 103

Peck A.B., Taylor G.B., Fassnacht C.D., Readhead A.C.S., Vermeulen R.C., 2000, ApJ, 534, 104

Ho L.C., Peng C.Y., 2001, ApJ, 555, 650

Pentericci L. et al., 2000, A&A, 361, L25

Petitjean P., Rauch M., Carswell R.F. 1994, A&A, 291, 29

Polletta M., Courvoisier T.J.-L., Hooper E.J., Wilkes B.J., 2000, A&A, 362, 75

Postman M, Lubin L.M., Oke J.B., 2001, AJ, 122, 1125

Proga D., Stone J.M., Kallman T.R., 2000, ApJ, 543, 686

Readhead A.C.S., Taylor G.B., Pearson T.J., Wilkinson P.N., 1996, ApJ, 460, 634

Reynolds C.S., 1997, MNRAS, 286, 513

Richards G.T., York D.G., Yanny B., Kollgaard R.I., Laurent-Muehleisen S.A., vanden Berk D.E., 1999, ApJ, 513, 576

Richards G.T., 2001, ApJS, 133, 53

Richards G.T., Laurent-Muehleisen S.A., Becker R.H., York D.G., 2001, ApJ, 547, 635

Röttgering H., Hunstead R.W., Miley G., van Ojik R., Wieringa M., 1995, MNRAS, 277, 389

Saikia D.J., Jeyakumar S., Salter C.J., Thomasson P., Spencer R.E., Mantovani F., 2001, MNRAS 321, 37

Sanders D.B., Soifer B.T., Elias J.H., Madore B.F., Matthews K., Neugebauer G., Scoville N.Z., 1988, ApJ, 325, 74

Shopbell P.L., Veilleux S., Bland-Hawthorn J., 1999, ApJ, 524, L83

Shull J.M., van Steenberg M.E., 1985, ApJ, 294, 599

Snellen I.A.G., Schilizzi R.T., Miley G.K., de Bruyn A.G., Bremer M.N., Röttgering, 2000, MNRAS, 319, 445

Sprayberry D., Foltz C.B., 1992, ApJ, 390, 39

Taylor G.B., Marr J.M., Pearson T.J., Readhead A.C.S., 2000, ApJ, 541, 112

Turnshek D.A., 1995, in QSO absorption lines, ed. G. Meylan (Berlin: Springer), 223

Turnshek D.A., Grillmair C.J., Foltz C.B., Weymann R.J., 1988, ApJ, 325, 651

Turnshek D.A. et al., 1994, ApJ, 428, 93

Tytler D., Fan X.-M., 1992, ApJS, 79, 1

Urry C.M., Padovani P., 1995, PASP, 107, 803

van Gorkom J.H., Knapp G.R., Ekers R.D., Ekers D.D., Laing R.A., Polk K.S., 1989, AJ, 97, 708

van Ojik R., Röttgering H., Miley G., Hunstead R.W., 1997, A& A, 317, 358

Vermeulen R.C., 2001, in ASP Conf. Ser. 199 'The Universe at low frequencies', eds V.K. Kapahi, A.P. Rao (San Francisco: ASP), in press (astro-ph/0012352)

Vernet J., Fosbury R.A.E., Villar-Martin M., Cohen M.H., Cimatti A., di Serego Alighieri S., Goodrich R.W., 2001, A&A, 366, 7

Vestergaard M., 2001, in 'Mass Outflow in AGN: New Perspectives', eds. M. Crenshaw, S.M. Kraemer, I.M. George, (San Francisco: ASP), in press (astro-ph/0109382)

Weymann R.J., 1995, in QSO absorption lines, ed. G. Meylan (Berlin: Springer), 213

Weymann R.J., Williams R.E., Peterson B.M., Turnshek D.A., 1979, ApJ, 234, 33

Weymann R.J., Morris SL., Foltz C.B., Hewett P.C., 1991, ApJ, 373, 23

Wold M., Lacy M., Lilje P.B., Serjeant S., 2000, MNRAS, 316, 267

Yee H.K.C., Green R.F., 1987, ApJ, 319, 28

Young P., Sargent W.L.W., Boksenberg A., 1982, ApJS, 48, 455

This 2-column preprint was prepared with the AAS LaTeX macros v4.0.

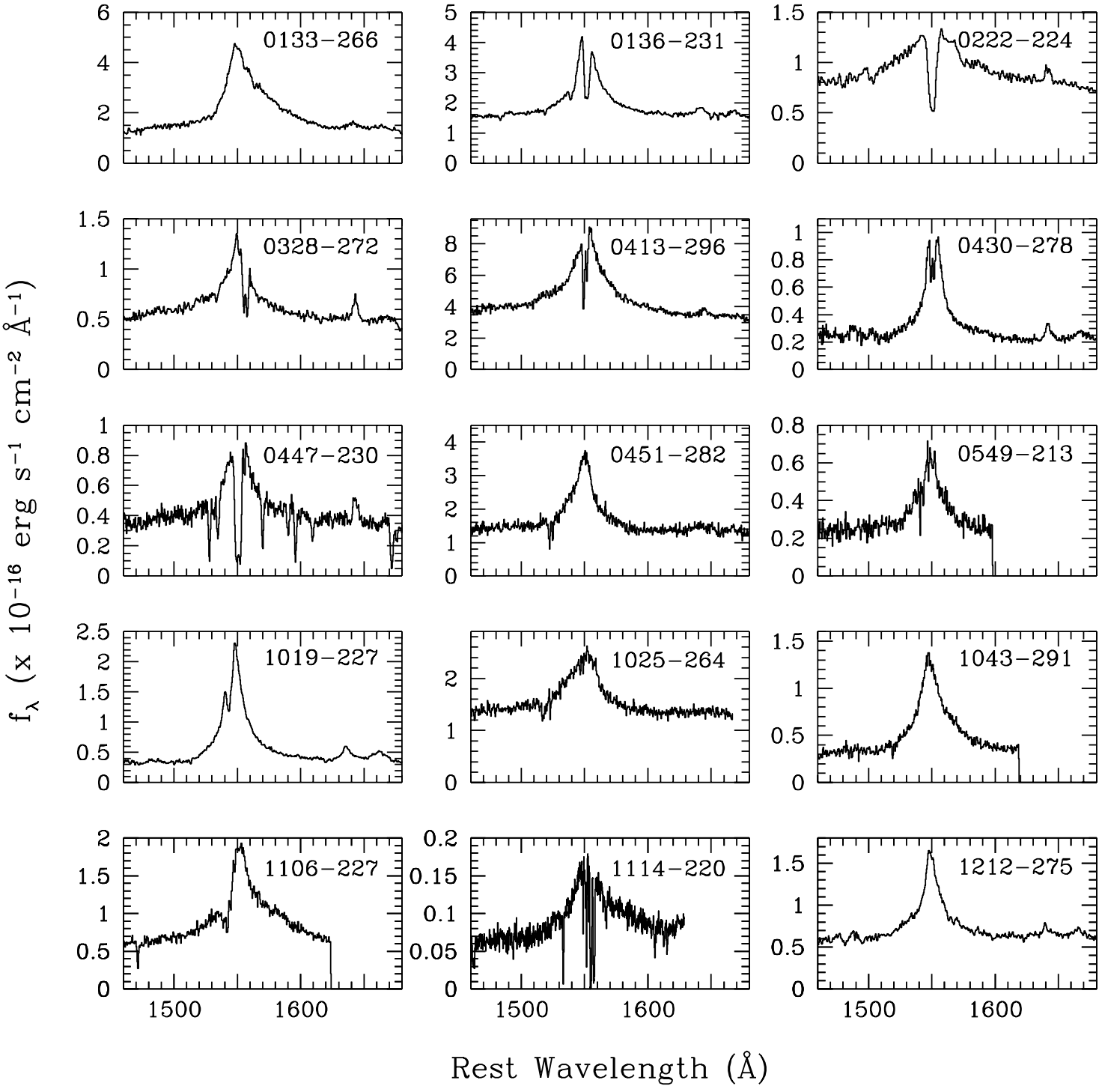

Fig. 1.— Spectra of C IV region (1400–1700Å) for $z > 1.5$ quasars observed from the ground.

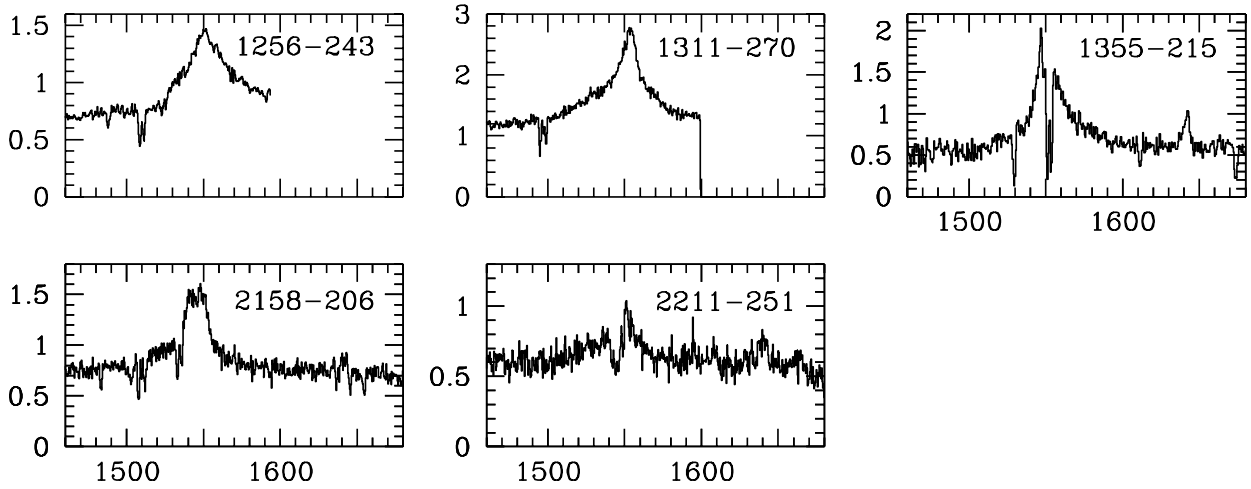

Fig. 1.— *Continued.* Spectra of C IV region (1400–1700Å) for $z > 1.5$ quasars observed from the ground.

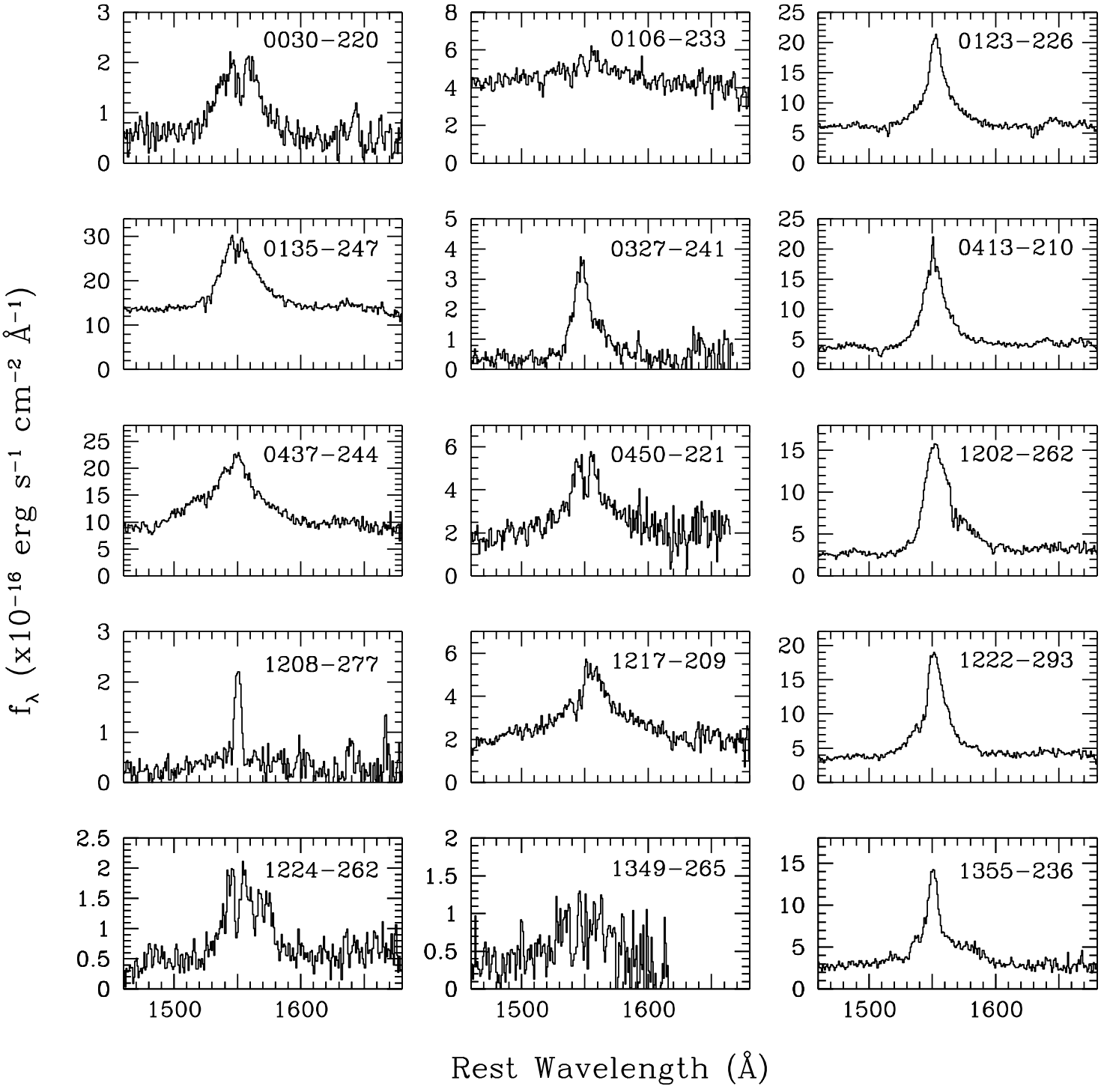

Fig. 2.— Spectra of C IV region (1400–1700Å) for $0.7 < z < 1.0$ quasars observed with HST.

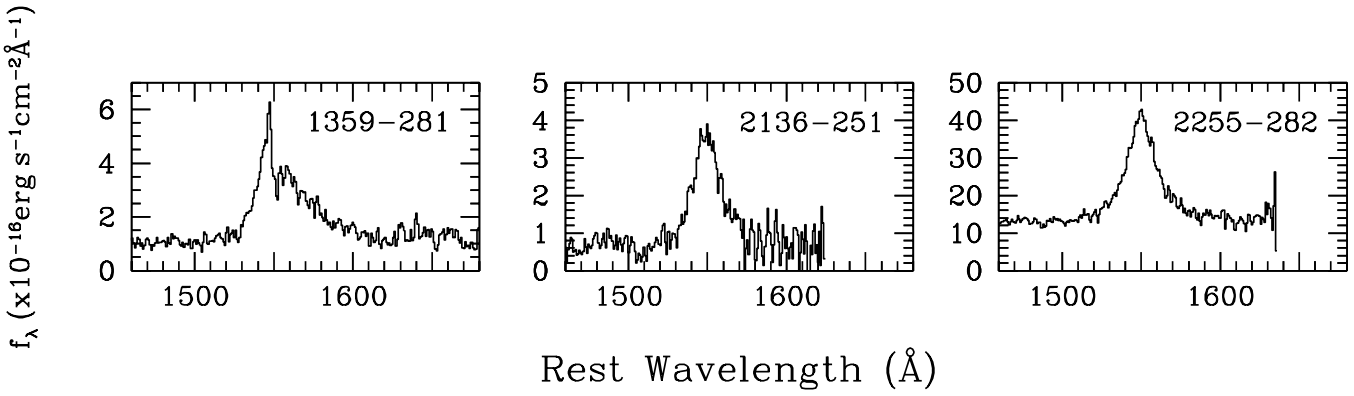

Fig. 2.— *Continued.* Spectra of C IV region (1400–1700Å) for $0.7 < z < 1.0$ quasars observed with HST.

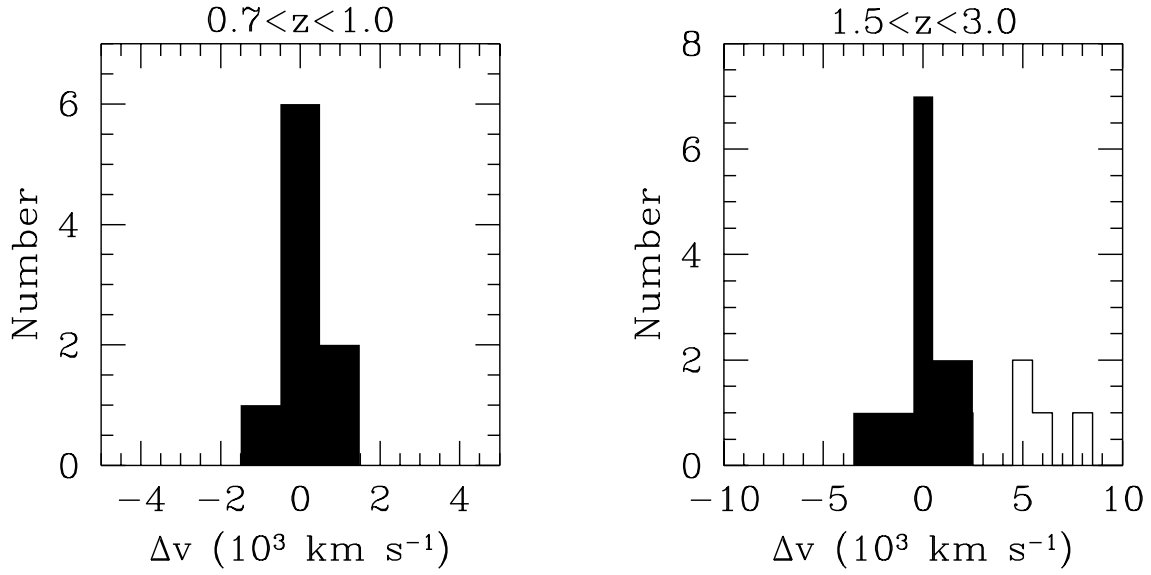

Fig. 3.— Histograms of velocities of the C IVλ1548 absorption line (or λ1550 blend) measured relative to the broad C IVλ1550 emission-line peak ($\Delta v = c(z_e - z_a)/(1 + z_e)$). Quasars with $0.7 < z < 1.0$ (HST observations) are shown on the left, those with $1.5 < z < 3.0$ (ground-based observations) on the right. Absorption lines with positive Δv are blueshifted with respect to the emission redshift. Systems with $|\Delta v| < 5000$ km s^{-1} are shaded.

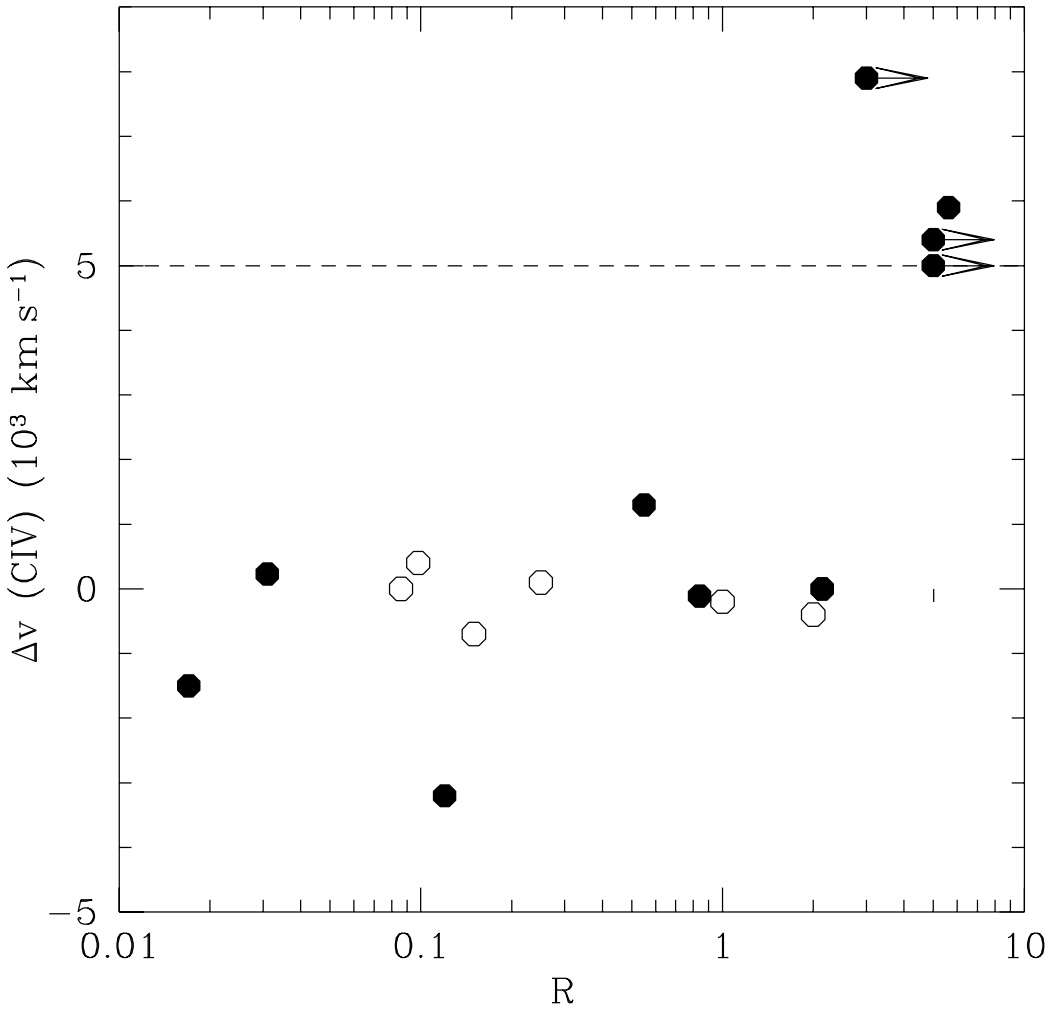

Fig. 4.— Relative velocity of C IV absorption as a function of radio core-to-lobe ratio, R (measured at 10-GHz in the restframe), for MQS quasars with $1.5 < z < 3.0$ (filled symbols) and $0.7 < z < 1.0$ (open symbols). Note all 4 quasars with $\Delta v \geq 5000\,\mathrm{km\,s^{-1}}$ absorption are very highly core dominated ($R > 3$).

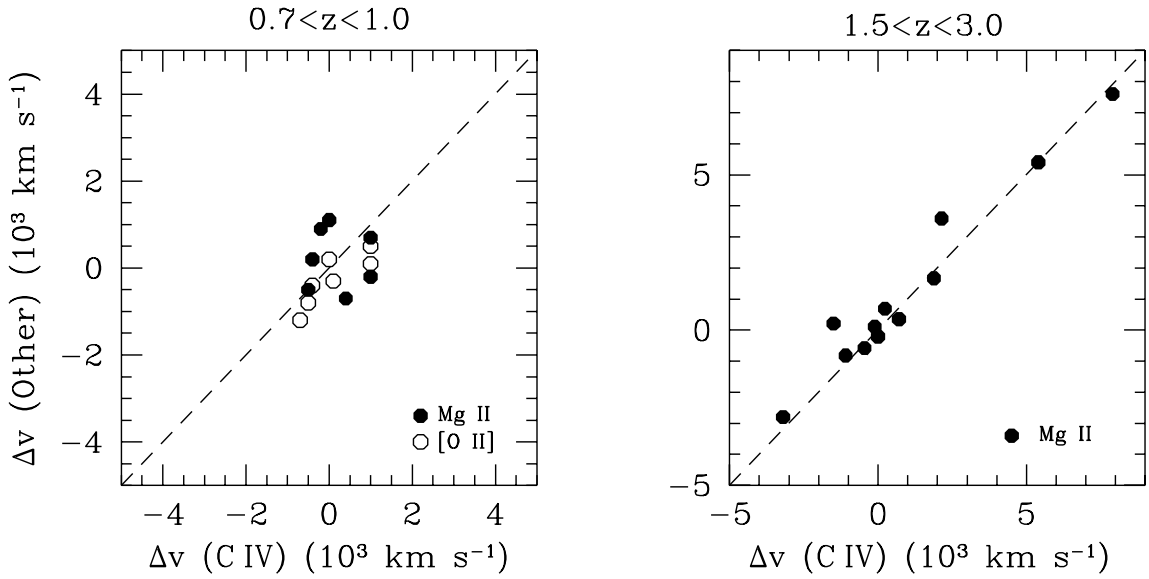

Fig. 5.— Comparison of velocities of the C IVλ1548 absorption line (or λ1550 blend) measured relative to the emission-line redshifts defined by the broad C IVλ1550 and Mg IIλ2800 (filled circles) or narrow [O II]λ3727 (open circles) emission lines for low- (*left*) and high- (*right*) redshift datasets. Measurements relative to [O II] are for $0.7 < z < 1.0$ quasars only. If there are no systematic shifts, then the points should scatter about the dashed lines, within the measurement uncertainties (see text).

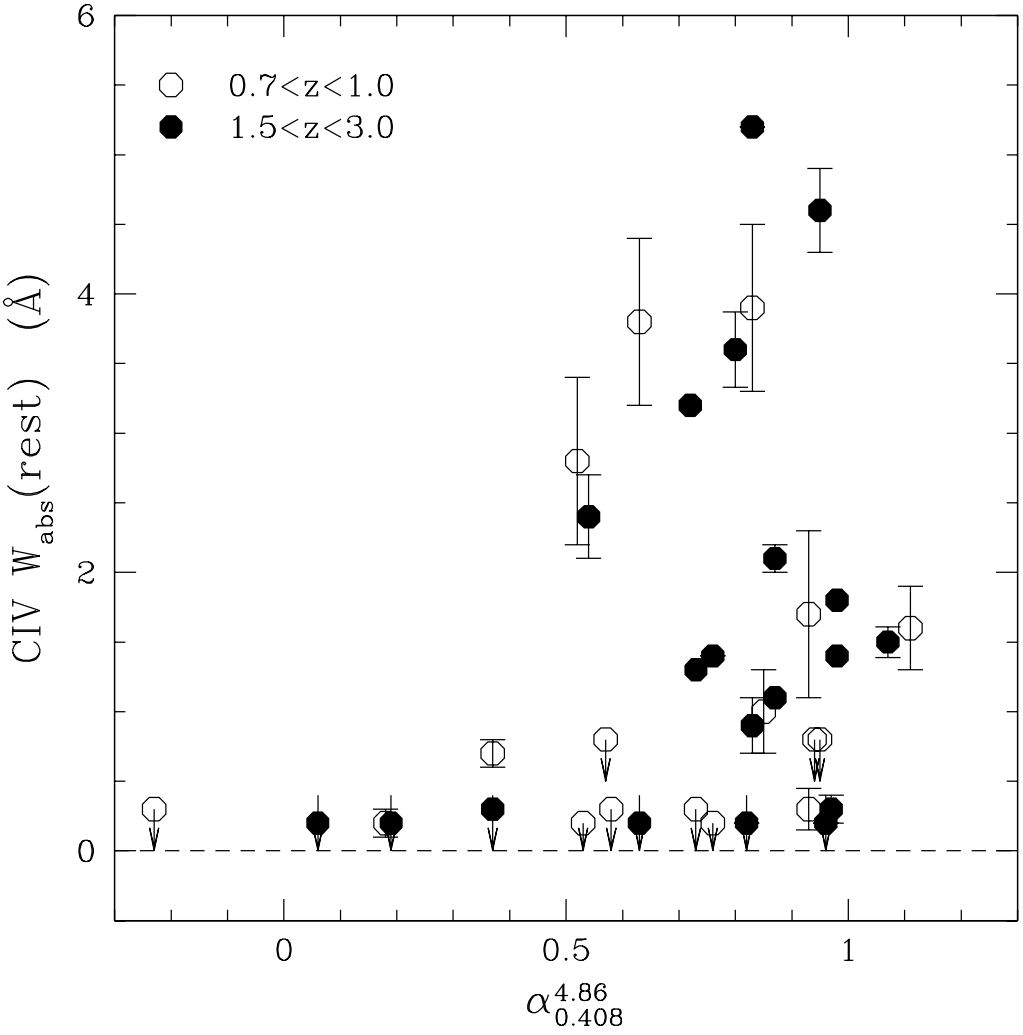

Fig. 6.— Equivalent width, $W_{\rm abs}$, of C IV$\lambda\lambda$1548,1550 absorption doublet ($\Delta v < 5000\,{\rm km\,s^{-1}}$) as a function of radio spectral index, $\alpha^{4.86}_{0.408}$ ($S_\nu \propto \nu^{-\alpha}$; measured between 408 MHz and 4.86 GHz), for MQS quasars. Quasars with $0.7 < z < 1.0$ are plotted as open circles, those with $1.5 < z < 3.0$ are plotted with filled symbols. Arrows indicate upper limits.

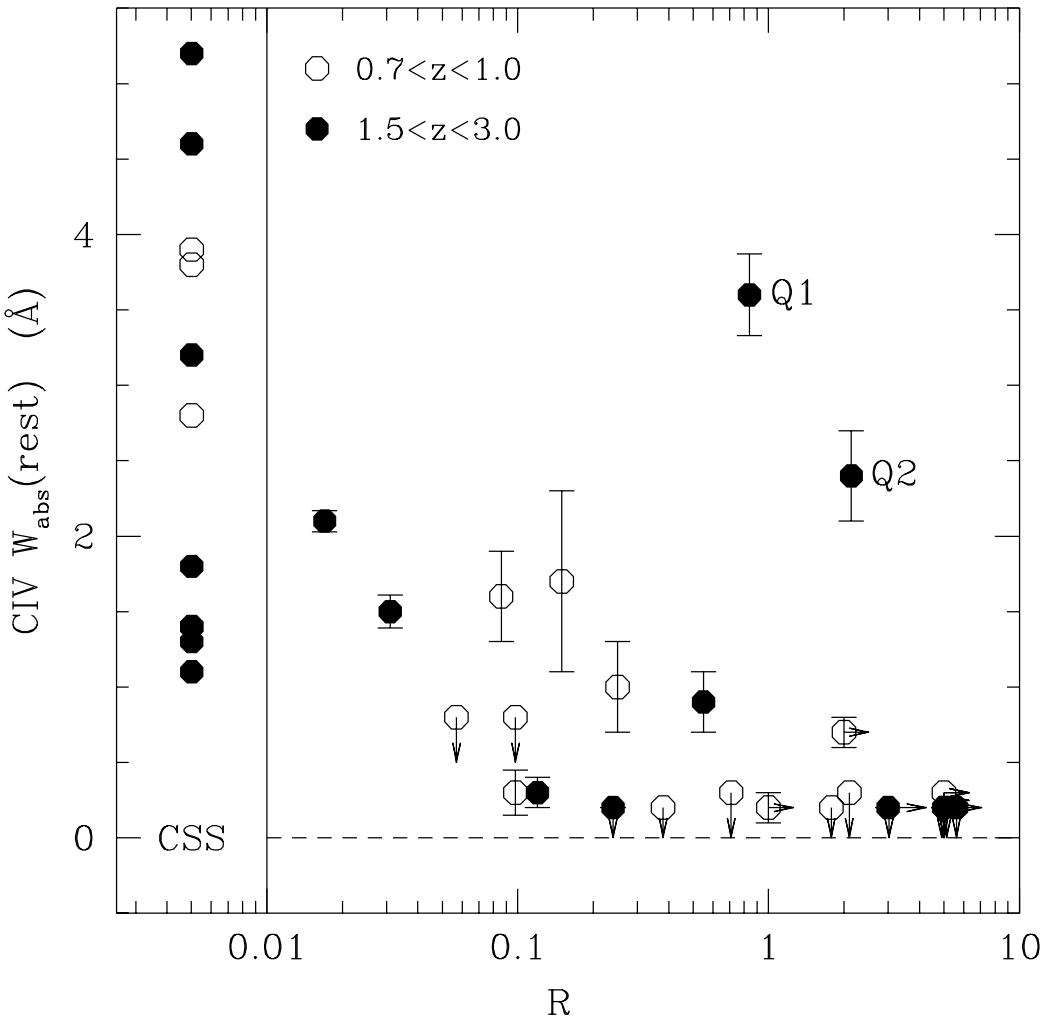

Fig. 7.— Equivalent width of C IV absorption as a function of radio core-to-lobe ratio, R. Quasars with $0.7 < z < 1.0$ (HST data) are plotted as open circles, those with $1.5 < z < 3.0$ are plotted with filled symbols. Limits are shown with arrows. Two outliers are labelled (see text), i.e. B1355–215 (Q1) and B0136–231 (Q2). CSSs do not have R measurements and are plotted separately on the left for comparison.

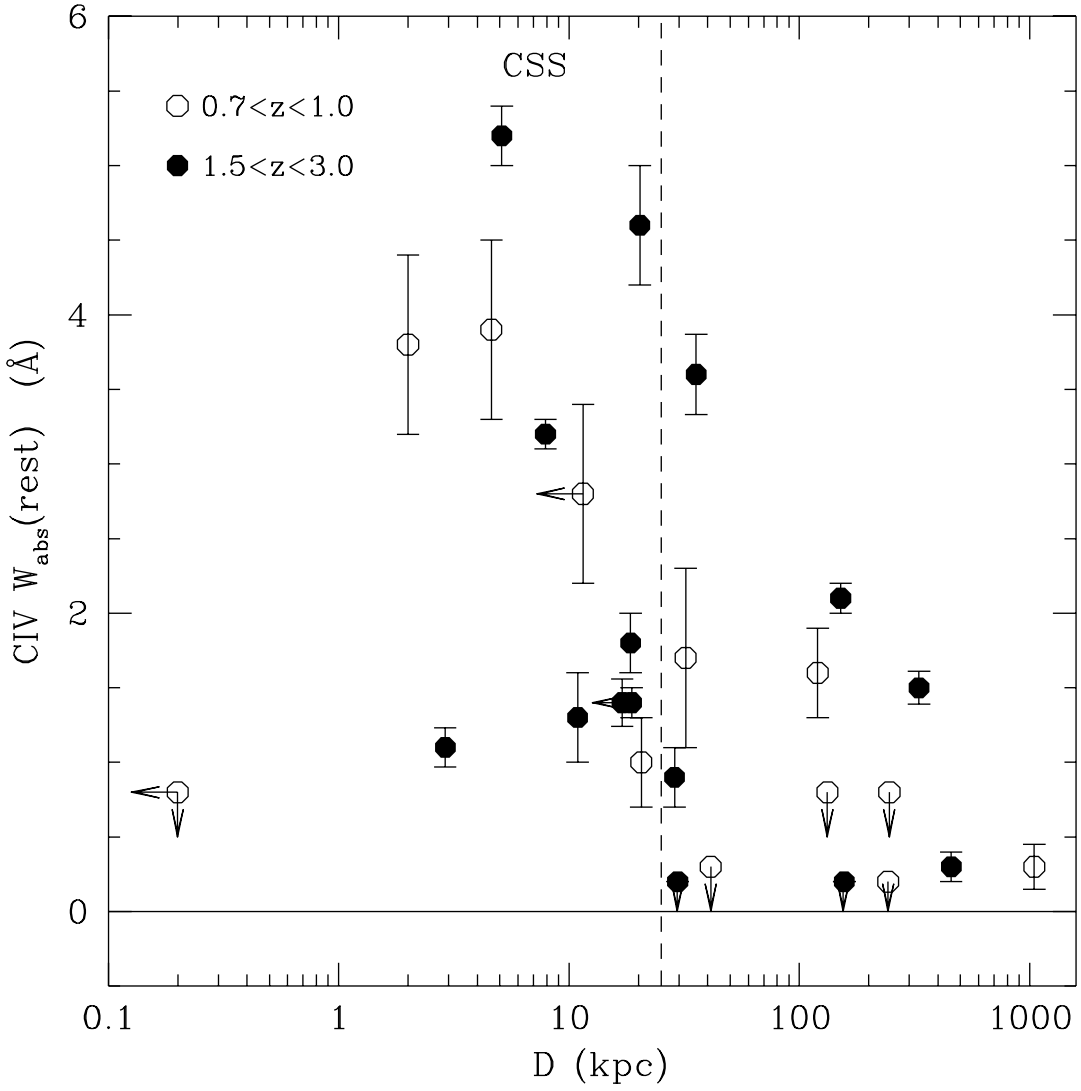

Fig. 8.— Equivalent width of C IV absorption as a function of radio source size, D (kpc). Quasars with $0.7 < z < 1.0$ are plotted as open circles, those with $1.5 < z < 3.0$ are plotted with filled symbols. The dotted line at $D = 25$ kpc illustrates the size limit used to define CSSs; we note this definition is somewhat arbitrary. The smallest quasar (< 0.2 kpc) is GPS source B2136–251.

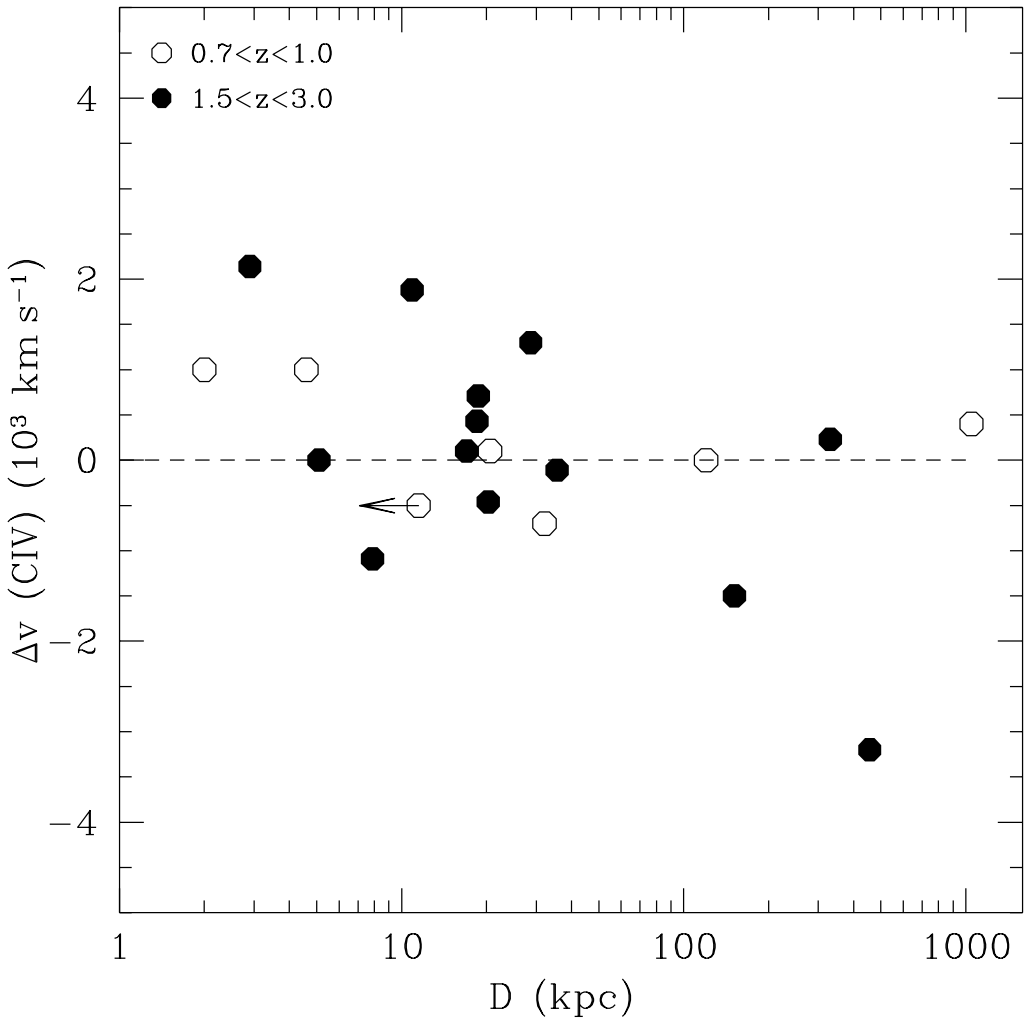

Fig. 9.— Velocity of narrow C IV absorption relative to broad C IV emission as a function of radio linear size (D). Positive absorption velocities are blueshifted with respect to the emission redshift. Quasars with $0.7 < z < 1.0$ are plotted as open circles, those with $1.5 < z < 3.0$ are plotted with filled symbols. Velocity uncertainties are roughly ± 600 km s^{-1}.

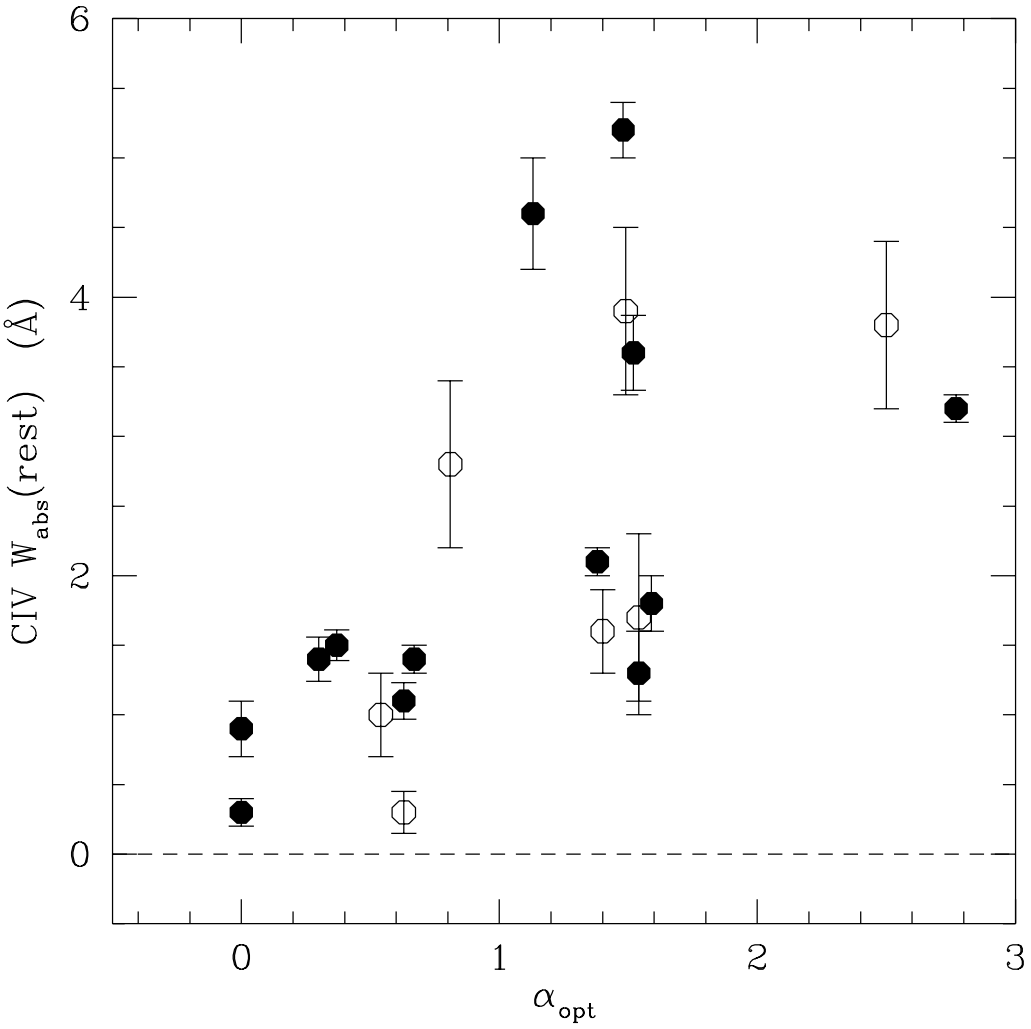

Fig. 10.— Equivalent width of C IV absorption doublet as a function of optical spectral index, $alpha_{opt}$ ($S_\nu \propto \nu^{-\alpha}$; measured between 4000 and 10000Å) for all quasars with detected absorption. Quasars with $0.7 < z < 1.0$ are plotted as open circles, those with $1.5 < z < 3.0$ are plotted with filled symbols.

Table 1: Observational data for all MQS quasars with $1.5 < z < 3.0$

MRC Quasar (1)	$\langle z_e \rangle$ (2)	b_J (3)	R (4)	D (kpc) (5)	α_{opt} (6)	$\alpha_{0.408}^{4.86}$ (7)	Tel (8)	UT Date (9)	Res (Å) (10)	Notes (11)
B0133–266	1.530	19.9	0.12	456.0	0.0	0.97	ESO	00-FEB-02	2.0	S
B0136–231	1.895	19.7	2.14	105.9	0.5	0.54	ESO	00-FEB-01	2.0	S
B0222–224	1.601*	19.1	CSS	20.3	1.13	0.95	ESO	00-FEB-01	2.0	S
							AAT	95-OCT-20	1.2	
B0237–233	2.224	16.4	GPS	< 0.1	0.64	0.05	AAT	95-OCT-19	1.2	Ly α only
B0246–231	2.914	21.4	CSS	< 1.8	1.92	0.70	AAT	95-OCT-19	1.2	Ly α only
B0328–272	1.803	18.1	0.017	151.1	1.38	0.87	ESO	00-FEB-01	2.0	S
B0413–296	1.608*	18.6	0.031	330.4	0.37	1.07	AAT	97-FEB-09	2.4	S
							ESO	00-FEB-02	2.0	
B0430–278	1.630	21.3	CSS	< 17.0	0.3	0.76	VLT	99-NOV-11,DEC-12	2.4	S
B0447–230	2.140	17.5	CSS	5.1	1.48	0.83	VLT	99-NOV-13,15	2.4	S
B0451–282	2.560	17.8	> 5	U	0.93	0.06	AAT	97-FEB-09	2.4	S
							AAT	99-APR-12	2.4	
B0522–215	1.820	22	CSS	15.3	1.66	1.00	...			
B0549–213	2.245	19.1	0.55	28.7	0.00	0.83	AAT	99-APR-11	2.4	S
							AAT	97-FEB-09	2.4	
B1019–227	1.550	21.1	CSS	18.7	0.67	0.98	ESO	00-FEB-02	2.0	S
							AAT	99-APR-11	2.4	
B1025–264	2.665	17.5	5.61	77.3	-0.7	0.63	AAT	97-FEB-09	2.4	S
B1043–291	2.128	18.6	> 5	8.0	1.52	0.19	AAT	99-APR-11	2.4	S
							AAT	97-FEB-09	2.4	
B1106–227	1.875	20.8	CSS	10.9	1.54	0.73	AAT	99-APR-11,12	2.4	S
							AAT	96-MAR-21,22	1.2	
B1114–220	2.282	20.2	CSS	7.9	2.77	0.72	AAT	96-MAR-21,22	1.2	S
							AAT	97-FEB-09	2.4	
							AAT	99-APR-11,12	2.4	
							VLT	99-DEC-11	2.4	
B1212–275	1.656	19.6	?	29.6	0.72	0.96	ESO	00-FEB-01	2.0	S
							AAT	97-FEB-09	2.4	
							AAT	99-APR-12	2.4	
B1256–243	2.263	17.6	> 3	65.2	1.41	0.37	ESO	00-FEB-01	2.0	S
							AAT	99-APR-11,12	2.4	
B1311–270	2.186	19.3	0.24	156.4	1.15	0.82	AAT	99-APR-11	2.4	S
B1355–215	1.604	19.9	0.84	35.6	1.52	0.80	AAT	99-APR-11,12	2.4	S
B2122–238	1.756*	17.8	0.50	13.4	0.76	0.71	...			
B2128–208	1.610	20.0	CSS	6.9	...	0.97	...			
B2158–206	2.249*	20.1	CSS	2.9	0.63	0.87	VLT	99-OCT-17,NOV-12	2.4	S
							AAT	95-OCT-20	1.2	Ly α
B2210–257	1.831	17.9	> 3	U	1.10	0.18	...			
B2211–251	2.500*	19.6	CSS	18.5	1.59	0.98	VLT	99-OCT-17,NOV-12	2.4	S
B2256–217	1.771*	19.9	0.085	277.8	1.31	1.2	...			

Columns— (1) name; (2) mean emission-line redshift measured from low-resolution spectra; (3) COSMOS UKST magnitude (b_J); (4) radio core-to-lobe luminosity ratio (measured at 10 GHz in the restframe), or classification as CSS or GPS; (5) radio linear size (D) in kpc (U=unresolved, beamed source); (6) optical spectral index (α_{opt}) as measured between 3500–10000Å; (7) radio spectral index, $\alpha_{0.408}^{4.86}$ measured between 408MHz and 4.86GHz; (8) telescope; (9) UT date of observations; (10) spectral resolution FWHM; (11) notes: where multiple spectra were obtained, 'S' denotes those spectra shown in Figure 1. The optical and radio data are taken from Kapahi et al. 1998 and Baker et al. 1999, except α_{opt} for 0447–230, 0451–282, 0522–215 and 1019–227 which are unpublished measurements from de Silva et al. (2001, in preparation).

* Redshift revised, since Baker et al. 1999

Table 2: MQS quasars with $0.7 < z < 1.0$ targetted with HST

MRC Quasar (1)	$\langle z_e \rangle$ (2)	b_J (3)	R (4)	D (kpc) (5)	α_{opt} (6)	$\alpha_{0.408}^{4.86}$ (7)	UT Date (8)	Time (s) (9)	Notes (10)
B0030–220	0.806	18.9	0.150	32	1.54	0.93	2000-Jun-20	5037	
B0106–233	0.818	20.1	0.25	21	0.54	0.85	2001-Feb-03	4738	
B0123–226	0.717	19.9	2.10	41	0.58	0.58	1999-Oct-16	4738	
B0135–247	0.835	18.9	> 2	...	0.31	0.37	2001-Feb-05	5037	
B0327–241	0.895	19.4	> 1	...	1.07	0.18	2000-Sep-20	4798	
B0413–210	0.807	18.4	0.71	41	1.60	0.73	1999-Sep-05	5053	
B0437–244	0.834	17.5	0.098	1050	0.63	0.93	1999-Aug-13	2206	
B0450–221	0.898	17.8	0.086	120	1.40	1.11	1999-Aug-16	2202	
B1202–262	0.786	19.8	1.78	123	1.32	0.53	1999-Jul-30	4772	
B1208–277	0.828	18.8	0.088	359	1.92	0.83	1999-Jun-28	5071	Narrow Ly α, C IV
B1217–209	0.814	20.2	0.057	246	0.17	0.94	1999-Aug-15	4738	
B1222–293	0.816	18.5	0.38	243	0.66	0.76	1999-Jul-30	5079	
B1224–262	0.768	19.8	CSS	5	1.49	0.83	1999-Aug-07	4772	
B1349–265	0.934	18.4	CSS	2	2.50	0.63	1999-Aug-20	5079	
B1355–236	0.832	19.9	0.098	133	1.17	0.95	1999-Jun-05	2198	
B1359–281	0.802	18.7	CSS	< 12	0.81	0.52	1999-Sep-07	5071	
B2136–251	0.940	18.1	GPS	< 0.2	1.97	0.57	1999-May-30	5057	
B2156–245	0.862	20.2	CSS	1.9	2.05	0.87	1999-Sep-11	4738	not detected
B2255–282	0.927	16.6	> 5	...	0.69	-0.23	1999-May-22	2223	

Columns— (1) to (7) as for Table 1; α_{opt} for B0437–244 was taken from de Silva et al. (2001, in preparation); column (8) UT date of HST observation; (9) total exposure time; (10) Notes.

Table 3: C IV emission and absorption measurements for $1.5 < z < 3.0$ MQS quasars

	Emission			Absorption					
MRC	CIV 1550		MgII 2800	CIV 1548		CIV	MgII	CIV (Å)	
quasar	λ_e (Å)	z_e	z_e	λ_a (Å)	z_a	Δv (km s^{-1})		$W_{\rm abs}$	$\Delta W_{\rm abs}$
(1)	(2)	(3)	(4)	(5)	(6)	(7)	(8)	(9)	(10)
B0133–266	3919	1.528	1.531	3955	1.555	−3200	−2800	0.3	0.1
B0136–231	4494	1.899	1.897	(4492)	1.899	0	−200	2.4	0.3
B0222–224	4030	1.600	1.599	(4032)	1.604	−450	−600	4.6	0.4
B0328–272	4343	1.802	1.818:	4360	1.816	−1500	200:	2.1	0.1
B0413–296	4049	1.612	1.616	4041	1.610	250	700	1.5	0.1
B0430–278	4081	1.633	...	4075	1.632	100	...	1.4	0.2
B0447–230	4870	2.142	...	4866	2.142	0	...	5.2	0.2
B0451–282	5516	2.559	...	...	...	...	...	< 0.2	...
				5419	2.500	5000*	...	0.9	0.2
B0549–213	5027	2.243	...	5000	2.229	1300	...	0.9	0.2
B1019–227	3948	1.547	1.544:	3934	1.541	700	350:	1.4	0.1
B1025–264	5679	2.664	2.592	...	...	...	...	< 0.2	...
				5561	...	5900*	...	0.6	0.2
B1043–291	4844	2.125	2.125	...	...	...	...	< 0.2	...
				4838	2.069	5400*	5400	1.3	0.3
B1106–227	4460	1.877	1.875	(4429)	1.859	1900	1650	1.3	0.3
B1114–220	5092	2.285	2.288	5104	2.297	−1100	−800	3.2	0.1
B1212–275	4114	1.654	1.645	...	...	...	...	< 0.2	...
B1256–243	5061	2.265	2.262	4922	2.179	7900*	7600	< 0.2	...
B1311–270	4949	2.194	...	...	...	...	...	< 0.1	...
B1355–215	4043	1.608	1.610	4039	1.609	−100	100	3.6	0.3
B2158–206	5022	2.240	2.256	4981	2.217	2150	3600	1.1	0.1
B2211–251	5412	2.492	...	(5405)	2.487	450	...	1.8	0.2

Columns— (1) MQS quasar; (2) Peak wavelength (λ_e) and (3) redshift (z_e) for C IVλ1550 emission line from these observations; (4) redshift for Mg IIλ2800 emission line from low-resolution spectra in Baker et al. (1999) (or de Silva et al. in prep., with colons); (5) Absorption wavelength and (6) redshift (λ_a, z_a) for C IVλ1548 line (or central wavelength of blended doublet given in parentheses); (7) & (8) velocity offset (Δv in km s^{-1}) of C IVλ1548 absorption line relative to the C IVλ1550 and Mg IIλ2800 emission lines, respectively (positive means absorption is blueshifted relative to emission); (9) restframe equivalent width W_λ of C IV doublet in absorption (or limits) and (10) measurement uncertainties (ΔW).

* $\Delta v \geq 5000$ km s^{-1}; velocity exceeds definition of associated absorption (see Section 4.1). An upper limit is also given for non-detection of associated absorption within 5000 km s^{-1}.

Table 4: C IV emission and absorption measurements for $0.7 < z < 1.0$ MQS quasars

	Emission				Absorption							
MRC	CIV 1550		MgII	[OII]	CIV 1548		CIV	MgII	[OII]	CIV (Å)		
quasar	λ_e(Å)	z_e	z_e	z_e	λ_a(Å)	z_a	Δv (km s^{-1})			$W_{\rm abs}$	$\Delta W_{\rm abs}$	
(1)	(2)	(3)	(4)	(5)	(6)	(7)	(8)	(9)	(10)	(11)	(12)	
B0030–220	2801	0.807	...	0.804	2804	0.811	−700	...	−1200	1.7	0.6	N
B0106–233	2821	0.820	...	0.817	(2820)	(0.819)	100	...	−300	1.0	0.3	
B0123–226	2667	0.721	0.715	0.720	...	...	...	...	...	< 0.3	...	
B0135–247	2842	0.834	0.837	0.834	2842	0.836	−400	200	−400	0.7	0.1	N
B0327–241	2931	0.891	0.898	...	2930	0.893	−200	900	...	0.2	0.1	
B0413–210	2802	0.808	0.809	0.807	...	...	...	...	...	< 0.3	...	
B0437–244	2839	0.832	0.825	...	2832	0.829	400	−700	...	0.3	0.15	
B0450–221	2944	0.899	0.906	0.900	2940	0.899	0	1100	200	1.6	0.3	
B1202–262	2772	0.788	0.789	...	...	...	...	...	...	< 0.2	...	N
B1208–277	2834	0.828	0.825	0.829	...	...	...	...	...	...	...	N
B1217–209	2821	0.820	0.816	...	...	...	...	...	...	< 0.8	...	
B1222–293	2816	0.817	0.817	0.820	...	...	...	...	...	< 0.2	...	
B1224–262	2751	0.775	0.773	0.772	2739	0.769	1000	700	500	3.9	0.8	N
B1349–265	2992	0.930	0.923	0.925	2979	0.924	1000	−200	100	3.8	0.6	N
B1355–236	2841	0.833	0.840	0.834	...	...	...	...	...	< 0.8	...	
B1359–281	2796	0.804	0.804	0.802	2797	0.807	−500	−500	−800	2.8	0.6	
B2136–251	3005	0.939	0.946	0.939	...	...	...	...	...	< 0.8	...	N
B2255–282	2987	0.927	0.919	0.925	...	...	...	...	...	< 0.3	...	

Columns— as Table 3, with addition of z_e [O II] (Col. 5) and Δv (Col. 10) relative to the redshift defined by the narrow [O II]λ3727 emission line (visible in optical spectra, Baker et al. 1999, de Silva et al., in prep.). N=notes in text.

Table 5: Statistics of strong absorbers in three quasar types

	CSS			LSS			CFS		
	low-z	high-z	Comb	low-z	high-z	Comb	low-z	high-z	Comb
Median $W_{\rm abs}$(Å)	3.3	1.6	2.8	< 0.8	0.9	< 0.8	0.2	< 0.2	< 0.3
N(total)	4	8	12	10	9	19	3	3	6
$N(W_{\rm abs} > 1$Å)	3	8	11	4	4	8	0	0	0
% ($W_{\rm abs} > 1$Å)	75	100	92	40	44	42	0	0	0

Columns— the quasars have been divided into three types: compact steep-spectrum (CSS : $D < 25$ kpc and $\alpha_{\rm rad} > 0.5$; as measured between 408 MHz and 4.86 GHz, and where $S_\nu \propto \nu^{-\alpha}$), large steep-spectrum (LSS : $D > 25$ kpc and $\alpha_{\rm rad} > 0.5$), and compact flat-spectrum (CFS : $\alpha_{\rm rad} < 0.5$, all are compact sources with $D < 25$ kpc). Statistics are given for the low-redshift ($0.7 < z < 1.0$), high-redshift ($1.5 < z < 3.0$) and combined samples.
Rows— the following for each type: median equivalent width, $W_{\rm abs}$; number of quasars with $W_{\rm abs} > 1$Å and total number of quasars of that type, N(total); and percentage of quasars with $W_{\rm abs} > 1$Å.